Integration of GNSS and BLE Technology With Inertial Sensors for Real-Time Positioning in Urban Environments

HUAN LUO[1,2]**, YAXIN LI**[1,2]**, JINGXIAN WANG**[2]**, DUOJIE WENG**[2]**, JUNHUA YE**[3]**, LI-TA HSU**[4]**, AND WU CHEN**[1,2]

[1]Shenzhen Research Institute, The Hong Kong Polytechnic University, Shenzhen, China
[2]Department of Land Surveying and Geo-Informatics, The Hong Kong Polytechnic University, Hong Kong
[3]College of Geological Engineering and Geomatics, Chang'an University, Xi'an 710054, China
[4]Interdisciplinary Division of Aeronautical and Aviation Engineering, The Hong Kong Polytechnic University, Hong Kong

Corresponding author: Yaxin Li (16902456r@connect.polyu.hk)

ABSTRACT The global navigation satellite system (GNSS) is widely used in smartphone positioning, but its performance can be degraded in urban environments because of signal reflections or blockages. To address these GNSS outages, pedestrian dead reckoning (PDR) is commonly used due to its significant improvements in both the stability and continuity of positioning, which are dependent on three key factors: continuous absolute position, heading and step information. Signals of opportunity are commonly used in positioning, whereas the installation of Bluetooth low energy (BLE) sensors on lampposts can provide an opportunity for positioning and heading estimation in urban canyons. In this article, a system integrating the GNSS, PDR, and BLE techniques is implemented in smartphones to provide a real-time positioning solution for pedestrians, which includes a new position correction method based on BLE heading, a reliable heading estimation integrating BLE and inertial sensors, an unconstrained step detection method with high accuracy, and an extended Kalman filter (EKF) to integrate multiple sensors and techniques. In several field experiments, with improvements in availability and robustness, the heading accuracy of the proposed fusion approach could reach approximately 3 degrees; the positioning accuracy achieved between 2.7 m and 4.2 m, compared with a 30 m error from the GNSS alone. Simultaneously, this system could achieve a high positioning accuracy of 2.4 m with unconstrained smartphones in a mixed environment. The proposed system has been demonstrated to perform well in urban canyons.

INDEX TERMS BLE, EKF, GNSS, heading estimation, PDR, positioning.

I. INTRODUCTION

In recent years, location-based service (LBS) has been an essential part of daily life, whether for mobile mapping, pedestrian navigation, intelligent travel, or emergency caller location [1]–[4]. Smartphones have become the most commonly used platform for LBSs owing to advances in processing capability along with self-containing inertial sensors and wireless signal communication systems. The global navigation satellite system (GNSS) is the most commonly used technology in smartphones, providing up to meter-level

The associate editor coordinating the review of this manuscript and approving it for publication was Venkata Ratnam Devanaboyina.

positioning in open-sky areas. However, this positioning accuracy can be degraded up to tens or hundreds of meters in deep urban canyons due to signal reflection and blockage [5]. To improve the positioning accuracy in urban areas, several methods for improving GNSS performance or integrating the GNSS with other technologies have been proposed, including multipath mitigation, map-aided methods, vision-based methods, signals of opportunity, and pedestrian dead reckoning (PDR) [6]–[17]. However, map-aided methods are impractical in areas lacking 3D maps or raster maps. The accuracy of the radio access network (RAN) is inadequate for high-precision positioning. Radio frequency identification (RFID) technology and ultra-wideband (UWB) technology

H. Luo *et al.*: Integration of GNSS and BLE Technology With Inertial Sensors for Real-Time Positioning in Urban Environments

IEEE *Access*

are unavailable in large areas because of the requirement of additional hardware installation. The positioning algorithms based on Wi-Fi technology are usually labor- and time-intensive. Among those methods based on signals of opportunity, the Bluetooth low energy (BLE) technique has the potential to provide positioning solutions due to easy installation and low-cost devices. In addition, owing to the construction of smart cities, a BLE signal system has been installed on lampposts (Fig. 1) for broadcasting in the multi-functional smart lampposts pilot scheme planned by the Hong Kong SAR government. The availability of BLE signals provides an opportunity to utilize them for positioning in urban canyons. With the built-in inertial sensors, PDR technology, which is effective to provide distance and heading propagation, is also widely applied to address GNSS outages [10].

FIGURE 1. A smart lamppost installed with iBeacon in Kowloon Bay, seen in the red rectangular.

GNSS is usually sufficient with high positioning accuracy in open area, which will not be discussed in this article. In urban environment, technologies, such as PDR and BLE, are commonly used to assist positioning due to the degraded GNSS measurements. Although several studies claimed that high accuracy positioning can be achieved by applying BLE alone [18], [19], the requirement of high density of device installation and/or high labor consumption makes it inapplicable in urban positioning. Considering the low installation density of iBeacon and environmental disturbances on signal strength outdoor, BLE technology is unable to provide continuous and reliable positioning solutions, and its positioning accuracy can only remain high in a limited effective range. Therefore, PDR technology is also essential to interpolate positions with high accuracy between GNSS and/or BLE outages.

PDR consists of three key components: step detection, step length and heading estimation [22]. For step detection, existing approaches can be categorized into three classes: machine learning methods, time domain-related methods, and frequency domain-related methods. Machine learning methods, such as hidden Markov models, k nearest neighbors (KNN) methods and K-means method, have been recently applied

to classify pedestrian activities, and steps can then be counted based on the distinguished gait phases [26]–[28]. However, they are labor intensive due to the requirement of a large amount of experimental data for training. Time- and frequency- domain-related methods detect steps based on the time series and spectrum series of inertial sensors, respectively. Time domain-related approaches include threshold-based [29], [30], peak detection [13], [31], [32], zero-crossing [33], [34] and correlation-based methods [35], [36]. These methods are usually limited to constrained sensors or smartphones (referring to the smartphone in a fixed position and hold style) [37], whereas frequency domain-related methods usually obtain the walking frequency based on fast Fourier transform (FFT) [37]–[39] and wavelet transform [40], which are not affected by the smartphone's position. Researchers have validated the feasibility of frequency domain analysis in extracting the walking mode or speed of pedestrians [38], [39]. Kang *et al.* [37] applied FFT to count steps for different situations based on the multiplication of the detected walking frequency and duration with an accuracy of 95.74%. However, the high accuracy requirement for step detection, which presents great challenges under unconstrained conditions, is one of the key problems to be resolved in this article. Step length is related to the step frequency, acceleration value within each step, walking speed and user height [22]. Since reliable estimation algorithms already exist, such as constant [10], [41], linear [42], [43], nonlinear [44], and artificial intelligence (AI) models [45], [46], this will not be discussed further here.

Smartphone headings are usually obtained from two types of inertial sensors: accelerometer and magnetometer, and gyroscopes. The use of accelerometers and magnetometers is unstable and inaccurate due to magnetic disturbances in urban environments [47]. Caruso considered iron effects from car bodies and reduced these effects [48]. This method requires external magnetic information, which is impractical in urban environments [46]. For the use of gyroscopes, it is necessary to obtain an absolute heading to initialize the heading and correct the error accumulation over time, however, the absolute heading obtained from low-cost microelectron mechanical systems (MEMSs) embodied in smartphones is not sufficiently accurate. Some studies have integrated gyroscopes with other sensors, techniques, or external information, such as the GNSS, acceleration, external sensors, and building headings [9], [49]–[52]. Nevertheless, these methods, which rely on external building heading or map information, are not suitable in the absence of a map source. Due to integration with the GNSS, the positioning accuracy is not sufficient in deep urban canyons. Some methods have been proposed to estimate the walking heading by analyzing acceleration and/or gyroscope data, such as principal component analysis (PCA), forward and lateral accelerations modeling (FLAM) and frequency analysis of inertial signals, independent of the smartphone orientation [53]–[56]. However, only specific possible of hand movement features were considered in those

IEEE *Access*

H. Luo *et al.*: Integration of GNSS and BLE Technology With Inertial Sensors for Real-Time Positioning in Urban Environments

methods, which suffered from numerous outliers [57]. In our previous study [13], a method based on the BLE technique was proposed to estimate pedestrian headings. However, the BLE heading was unstable because of signal unavailability due to limited coverage, so the fusion of BLE heading and inertial sensor data was not robust using the sum between two orientations. Improvement of the heading estimation is required to ensure the precision and robustness of pedestrian headings.

Several existing methods can be applied to integrate inertial sensors with the GNSS and/or wireless network signal, including the particle filter (PF), Kalman filter (KF), extended Kalman filter (EKF), unscented Kalman filter (UKF), federated filter (FF) and strong track Kalman filter (STKF) [58]–[64]. The PF has great advantages in nonlinear or non-Gaussian systems [58]. However, its performance depends on the number of particles, which means that a higher computational complexity is necessary to achieve a good estimation [65]. The KF, which is an optimal approach to address linear Gaussian state-space models, has been widely applied in position estimation [65]. However, the KF is unsuitable to integrate PDR with the GNSS and/or wireless network signals since the PDR is a nonlinear system. Relative to the KF, the EKF and UKF are used in nonlinear systems, whereas the EKF is based on linearization of the state-space equation around the updated values of state variables, and the UKF utilizes the nonlinear unscented transformation (UT) of sigma points [60]. When dealing with a highly nonlinear system, the UKF can achieve higher accuracy than the EKF. For normal nonlinear systems, the EKF also performs well. Karimi *et al.* proved that the EKF is better than the UKF in the integration system of a Doppler velocity log (DVL) and an inertial navigation system (INS) [60]. The STKF introduces a fading factor into the prediction error covariance matrix to overcome the problem that the traditional KF requires the precise prior knowledge of the process noise and the measurement noise [63], but the determination of the fading factor heavily relies on personal experience or computer simulations using a searching scheme. Considering the increase in the use of multi-sensors, FF is widely used to obtain accurate navigation solutions based on the distributed filter structure [64]. However, an FF will increase the computational complexity, and it is not necessary to use an FF when the number of sub-systems is small. Among these filters, the EKF is more computationally efficient [66]. When the information of system models and noise types are demonstrated with high accuracy, positioning performance can be guaranteed in integration using the EKF.

The EKF has been applied to provide real-time positioning solutions in urban canyons in Hong Kong. Our previous work mainly focused on validating its feasibility through field experiments [13]. However, further research is required in terms of the integration algorithm, such as the limitation with constrained smartphones; the instability of positioning and heading estimation, etc. Based on our previous algorithm, the step detection is improved to count steps under

unconstrained conditions. The heading estimation based on the BLE technique is improved to correct the bias caused by walking dynamics, and the proposed method further ensures the robustness and availability of the system. Meanwhile, a new positioning correction method with a BLE heading is proposed to improve the positioning accuracy. To guarantee the performance of the integrated system, we first assess the performance of the step detection, heading estimation and positioning correction methods, and then several field experiments are carried out to evaluate the performance of the whole integration system.

The rest of this article is organized as follows: a brief introduction and methodology of the proposed system are presented in Section 2. Section 3 illustrates the detailed experiments for each component of the system and compares the positioning results derived from different methods. The conclusion and future works are summarized in the last section.

II. INTEGRATION METHODOLOGY AND ALGORITHMS

In our integration system, the BLE and GNSS are used to provide positioning solutions, and PDR is applied as the propagation part to fill the gap of BLE and/or GNSS outages. A loosely coupled EKF is then used to integrate these techniques.

A. PEDESTRIAN DEAD RECKONING ALGORITHM

PDR is fundamental to the whole integration system, including step detection, step length and heading estimation.

1) STEP DETECTION

Generally, step detection is based on the analysis of specific force data [67]. The waveform of the accelerometer represents the walking pattern of a pedestrian. In this article, the FFT, which is widely used to analyze the frequency characteristics of time series data, is adopted to detect the step.

The FFT is applied on single axis of acceleration data since the sum of the three axes changes the frequency features. As discussed by Kang *et al.* [37], the sensitive axis is selected based on the maximum magnitude since smaller measurements are prone to be affected by noise, expressed as:

$$sa = \underset{a=x,y,z}{arg\,max} \sum_{i=1}^{TW} |\omega_a(i)| \qquad (1)$$

where *sa* is the sensitive axis within the axis a with a = x, y, z, ω is acceleration on each axis, *TW* is size of time window, and *i* is the epoch within the current time window.

The acceleration on the sensitive axis is transformed to the frequency domain with FFT [68], expressed as

$$X_k = \sum_{i=0}^{TW-1} \omega_{sa}(i)\, e^{-j2\pi k \frac{i}{N}} \qquad (2)$$

where $k = 0, 1, \cdots, TW-1$, $\omega_{sa}(i)$ is the acceleration on the sensitive axis, and $j = \sqrt{-1}$.

H. Luo *et al.*: Integration of GNSS and BLE Technology With Inertial Sensors for Real-Time Positioning in Urban Environments

IEEE *Access*

The spectra of acceleration in six different activities during walking are then analyzed, as shown in Fig. 2.
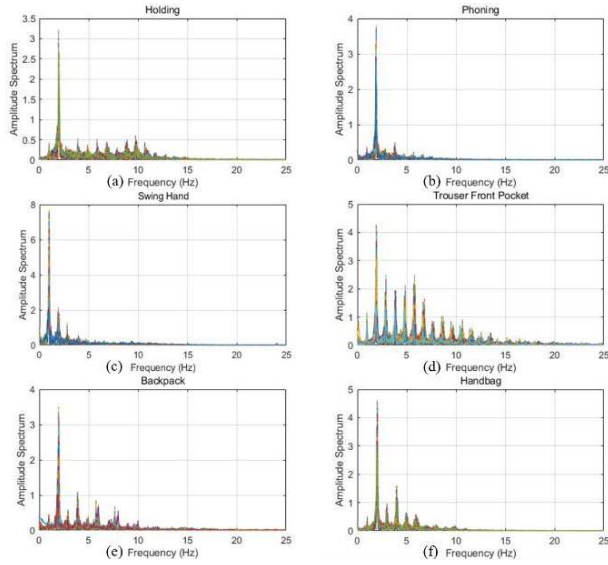

FIGURE 2. Spectrum analysis of acceleration in six activities, including holding, phoning, swing hand, trouser front pocket, backpack and handbag.

The acceleration frequency performances vary for different pedestrian activities. In Fig. 2, it can be observed that the frequency of normal walking ranges between 1.2 Hz and 2.2 Hz. Specifically, the frequency with the largest acceleration magnitude is approximately 0.95 Hz when a smartphone is held in the swing hand, which is actually the swing frequency of the hand since the acceleration amplitude of the hand swing is larger than that of walking, whereas the vice frequency is approximately 1.95 Hz, which is the walking frequency. When a smartphone is put or held in a relatively stable posture, such as holding and phoning, a main frequency can be distinctively observed, as its magnitude is much larger than that of other frequencies; when a smartphone is put in a free position, including a trouser pocket, backpack and handbag, there are several frequencies, but a main frequency with the largest magnitude can also be observed.

In Fig. 2, it can be observed that the walking frequencies ranges for different pedestrian activities during a long period, so an adaptive interval of cut-off frequency is applied to filter out the walking frequency. As mentioned above, the walking frequency approximately varies between 1.2 Hz to 2.2 Hz in experiments data. The mean, 1.7 Hz, is defined as the initial reference frequency with ±0.5 Hz cut-off range, hence, 1.2 Hz and 2.2 Hz. Based on the FFT, the frequency with maximum amplitude within the cut-off range will be extracted as the current reference frequency, otherwise, the initial reference frequency will be retained as current reference frequency. Then, the adaptive interval of cut-off frequency is set to be current reference frequency ±0.5 Hz. Applying the adaptive cut-off frequency interval in the FFT, the remaining frequency can be used to filter the angular

velocity data, as shown in Fig. 3(a), and the peak detection method is applied on the filtered data, as shown in Fig. 3(b).
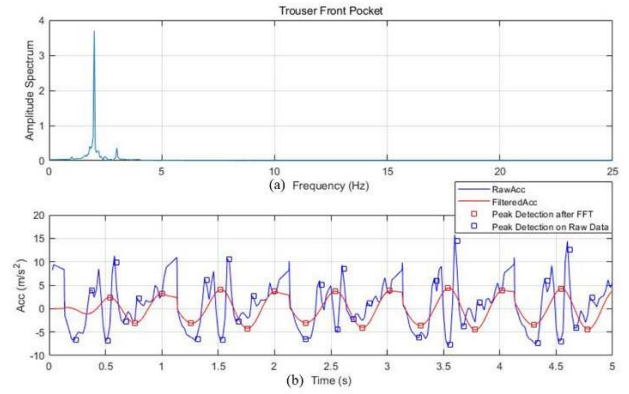

FIGURE 3. Step detection after filtering in the frequency domain: (a) Walking frequency determination after a bandpass filter; (b) Acceleration data filtered with the walking frequency and step detection.

In Fig. 3(a), the main walking frequency at approximately 2 Hz is determined and other frequencies are cut off compared with Fig. 2(d). In Fig. 3(b), the filtered data (red line) are smoother than the raw data (blue line), and the cyclic characteristics also remain in the filtered data. Compared to step detection on raw angular velocity data, step detection after filtering has a higher accuracy.

Based on the analysis above, step detection with FFT is proposed, as presented in Algorithm 1, where fft() is the function used to transform the acceleration data into the frequency domain, butter() is the function used to filter the frequency of acceleration data with a bandpass filter, and peakDetection() is the function used to detect peaks and valleys of filtered acceleration data to count steps. The pedometer is then implemented in the smartphone based on Algorithm 1.

2) STEP LENGTH ESTIMATION

As mentioned above, conventional empirical models perform well when estimating step length indoors, whereas their performance outdoors needs to be tested. In this article, three common models [43], [44] are selected for comparison, including the constant model, non-linear model proposed by Weinberg [44], and linear function proposed by Chen *et al.* [43], expressed in order as

$$\begin{cases} SL = H \cdot 0.4 \\ SL = K \cdot \sqrt[4]{(Acc_{max} - Acc_{min})} \\ SL = \left(0.7 + a\,(H - 1.75) + \dfrac{b\,(SF - 1.79)\,H}{1.75}\right) c \end{cases} \quad (3)$$

where SL is the step length, H denotes the user height in meters, Acc_{max} and Acc_{min} are the maximum and minimum acceleration within each step, K is a personal parameter, which is also related to devices, SF is the step frequency from step detection, a and b are constants of 0.371 and 0.227 respectively, and c is a factor related to individuals, which is close to 1.

Algorithm 1 Step Detection With FFT Transformation

Input: sampling frequency: F_s

Sampling period: $T_s = 1/F_s$

Time interval: T_i

Size of time window: $T_W = T_i \cdot F_s$

Walking frequency: F_W

Linear Acceleration: ω

Time end of Acceleration: T_e

Threshold of minimum walking frequency: T_{min}

Threshold of maximum walking frequency: T_{max}

Output: step number: SN

Initialization: $F_s = 50$; $T_i = 20$; $F_W = 1.7$

for $index = T_i$, $index \leq$ Te, $index + +$

    Linear acceleration data within time window: $\omega^{TW} = \omega(index - T_i: index)$

    Selection of sensitive axis ω_{sa} of linear acceleration data using (1) within ω^{TW}

    Frequency of ω_{sa} using FFT transform with (2): $F_\omega^{TW} = fft(\omega_{sa}, T_W)$

    Cut off frequency: $F_L = F_W - 0.5$; $F_H = F_W + 0.5$;

    Frequency cutoff of F_ω^{cut}: $F_\omega^{cut} = F_\omega^{TW}(f > F_L \& f < F_H)$

    Frequency with maximum amplitude F_ω^{max}: $F_\omega^{max} = argmax(A_f)$

    if $F_\omega^{max} > T_{min} \& F_\omega^{max} < T_{max}$

        Walking frequency: $F_W = F_\omega^{max}$

    else

        Walking frequency: $F_W = 1.7$

    end

    Filtered linear acceleration data using the bandpass filter: $\omega^{filtered} = butter(\omega_{sa}, F_L, F_H)$

    Step counts within time window: $SN^{TW} = peakDetection(\omega^{filtered})$

    Step counts in total: $SN + = SN^{TW}$

end

return SN

If the pedestrian crosses two iBeacon base stations directly, where no turn is detected (detailed analysis as follows), the step length can be corrected using the following equation:

$$SL = \frac{d_{p_i p_j}}{SN} \quad (0.55 < SL < 0.9) \quad (4)$$

where d indicates the distance between two neighboring lampposts, p_i and p_j, and SN is the step number between the two base stations.

Until the calculated SL is between the threshold, which is determined with experiments, the value is applied as the scale factor correction in EKF integration.

3) HEADING ESTIMATION

Generally, pedestrian behaviors can be classified into two types: walking along a street and turning at a street corner. When a pedestrian walks along a street, the absolute heading of the pedestrian approximately equals the street orientation.

If the pedestrian turns a corner, the heading can be determined based on the relative change in heading within the turning behavior and the heading along the street. Based on the street heading determination and turning detection and calculation, the pedestrian's heading can be estimated and propagated. In this article, the heading estimation includes three parts: street heading determination by BLE techniques, turning detection by a gyroscope and the fusion of heading from the BLE and gyroscope.

a: HEADING ESTIMATION FROM BLE

The basis of BLE heading estimation is built on the trend analysis of BLE signal strength, expressed as received signal strength indicator (RSSI). Theoretically, when the pedestrian crosses iBeacon 1 to neighboring iBeacon 2, the RSSI trend of iBeacon 1 will experience a drop while that of iBeacon 2 will experience a rise, as shown in Fig. 4(b), where eight iBeacon are installed on lampposts, and lines in different colors indicate the RSSI variations of different iBeacon. Since the position of each iBeacon is accurately known, the heading can be estimated by analyzing the variation in the RSSI of the neighboring iBeacon.

RSSI values are stable in static environments, but change significantly under dynamic conditions [69], [70], as shown in Fig. 4(a). The average filter is widely applied for RSSI purification since it achieves similar accuracy with other filters but has less computation burden [71]. Therefore, it is applied in this study. As shown in Fig. 4(b), the noise of RSSI values is largely reduced after filtering. The trend of RSSI values can be obtained to indicate whether the pedestrian gets close to or far away from the iBeacon. However, the trend might be inconsistent with the walking heading in some cases since the RSSI values fluctuate significantly in urban areas, as shown by the black ellipse in Fig. 4(b). Meanwhile, the distance between neighboring iBeacon varies depending on the location of the lampposts, as indicated by the red dotted line in Fig. 4; thus, the distance of trend
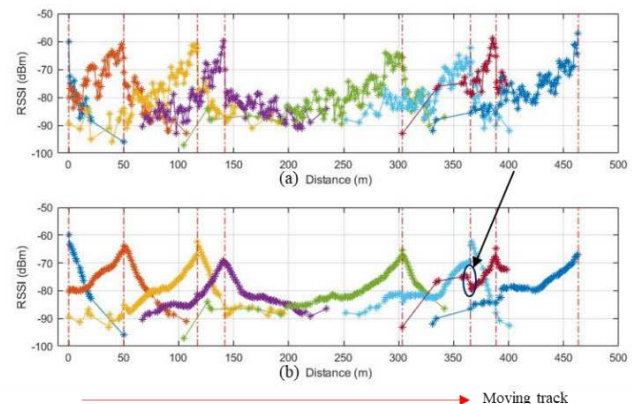

FIGURE 4. Variation in RSSI values with distance when a pedestrian crosses iBeacon; (a) Raw RSSI values; (b) Filtered RSSI values. The red dotted line indicates the locations of the iBeacon, and colored lines represent RSSI values from different iBeacon.

H. Luo *et al.*: Integration of GNSS and BLE Technology With Inertial Sensors for Real-Time Positioning in Urban Environments

IEEE *Access*

occurrence for the iBeacon with one transmission power (TP) might be out of the effective range, which would fail to detect the heading. To solve the above problems, three iBeacon with different TPs, including weak, middle and strong TPs, are installed on each location as one base station.

The detailed flowchart of BLE heading estimation is shown in Fig. 5. It consists of three parts: iBeacon detection, indicator calculation and heading determination. In the iBeacon detection part, the program scans the iBeacon, and a list of received RSSI values is saved and filtered dynamically. Slopes of the RSSI value are then calculated. The indicator of iBeacon, which is used to indicate whether the RSSI values increase or decrease, is determined with the slope by comparison with the preset slope threshold empirically derived from tests, expressed as

$$\begin{cases} Ind = 1 \ (Slope_{iB} > Slope_{increase}) \\ Ind = -1 \ (Slope_{iB} < Slope_{decrease}) \end{cases} \tag{5}$$
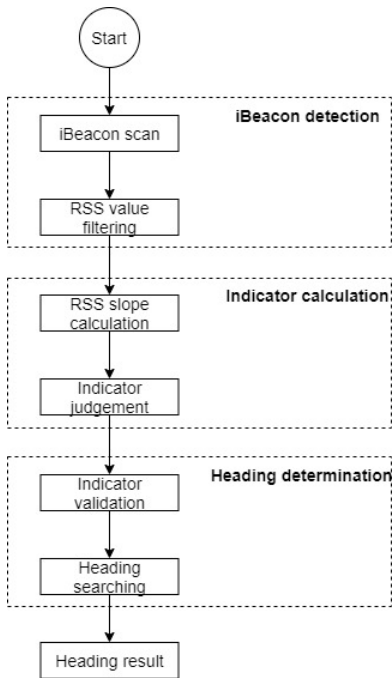

FIGURE 5. Flowchart of the proposed street heading determination using multiple classes of iBeacon on a single lamppost.

where *Ind* is the slope indicator of iBeacon, $Slope_{iB}$ is the slope of RSSI list, and $Slope_{increase}$ and $Slope_{decrease}$ are the threshold of slope for increasing and decreasing RSSI values, respectively.

In the heading determination part, two validation steps are conducted to ensure the correctness of heading estimation: a validation of indicator determination between three TP iBeacon and a validation of indicator searching between all estimated headings. After passing validation, the BLE heading is then determined based on the heading map of iBeacon,

expressed as

$$\begin{cases} \theta^{BLE} = \theta_{iB_{ij}} \ (Ind_i = -1, Ind_j = 1) \\ \theta^{BLE} = \theta_{iB_{ij}} + 180° \ (Ind_i = 1, Ind_j = -1) \end{cases} \tag{6}$$

where θ^{BLE} is BLE heading, $\theta_{iB_{ij}}$ denotes the heading searched from the heading map, which is the heading orientating from *i* to *j*.

b: TURNING DETECTION

A gyroscope is a sensor used to obtain the relative heading of a device within a sampling interval and is sensitive to angular changes. The accuracy of the gyroscope data integral over a short time window is high, so the integral can be used to detect the turning of the pedestrian, which helps to indicate the movement of the pedestrian, e.g. whether he/she walks in a straight line or turns at a corner.

The relative heading change of a given period is estimated from the gyroscope, which is expressed as

$$\Delta \Omega_i = \int_1^n r_i dt = \sum_1^n r_i \Delta t \tag{7}$$

where *r* is the angular velocity, and Δt is the sampling interval of the gyroscope outputs.

For normal walking, the heading of pedestrians can change in four ways, as shown in Fig. 6. When the pedestrian walks straightly on the street, the walking heading might remain the same or experience a peak caused by pedestrian avoidance, as shown in Fig. 6(a) and Fig.6(b) respectively. When the pedestrian turns a corner, the walking heading might increase or decrease (Fig. 6(c) and Fig. 6(d)). In our previous research [13], the turning angle is determined by the calculation of the maximum gyroscope integral within a time window. However, the calculation of turns caused
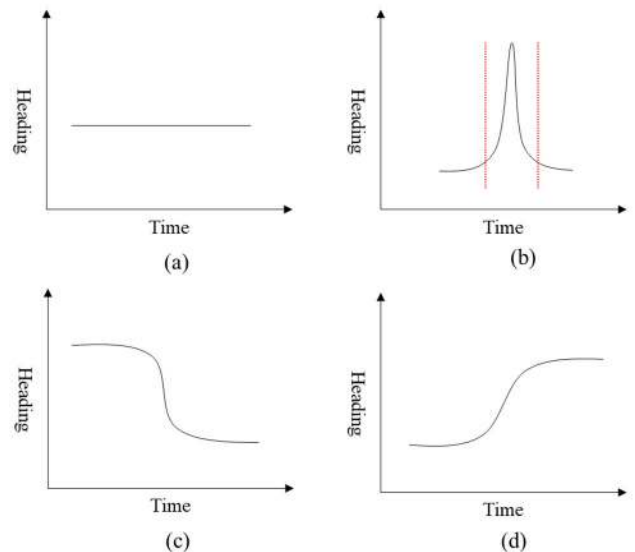

FIGURE 6. Illustration of the heading variation when pedestrians walk in a normal situation.

by pedestrian avoidance is incorrect (Fig. 6(b)), where the headings are the same before and after turning.

In this article, the turning detection algorithm is improved and expressed as follows:

$$
\begin{cases}
\Delta H_i = max \, |\Delta \Omega_m - \Delta \Omega_{m-TW}| \\
\Delta H_i^{TW} = |\Delta \Omega_i - \Delta \Omega_{i-2TW}|
\end{cases} \tag{8}
$$

where i is the current epoch, TW is the time window indicating turning completion, which is set as 3 seconds, m indicates the epoch between $i - 2TW$ and i, ΔH_i is the maximum gyroscope integral within the time window, and ΔH_i^{TW} is the gyroscope integral within two time windows.

Referring to (8), the turning type, corresponding to the four situations in Fig. 6, can be determined by comparing ΔH_i and ΔH_i^{TW} with the turning threshold, as shown in Table 1, and then the turning angle can be calculated.

TABLE 1. Turning type determination.

Turning type	ΔH_i	ΔH_i^{TW}
a	0	0
b	> H_T	0
c	> H_T	> H_T
d	> H_T	> H_T

[a] H_T represent the threshold of the turning angle. If the gyroscope integral is larger than the threshold, the integral is considered the turning angle.

c: HEADING INTEGRATION

In our previous research [13], if no turn is detected within the duration of heading estimation based on BLE as shown in Fig. 6(a), the heading from BLE will be used as the current heading. If a turning is detected, the heading will be updated by the absolute heading in the last epoch and the turning heading detected by the gyroscope. However, for the gyroscope integral shown in Fig. 7 when the pedestrian walks on a street, the main heading is shown as the red line, and the real orientation of phone are shown as the blue line, as estimated from the gyroscope. The heading from BLE will be estimated at any epoch, which represents the main heading,
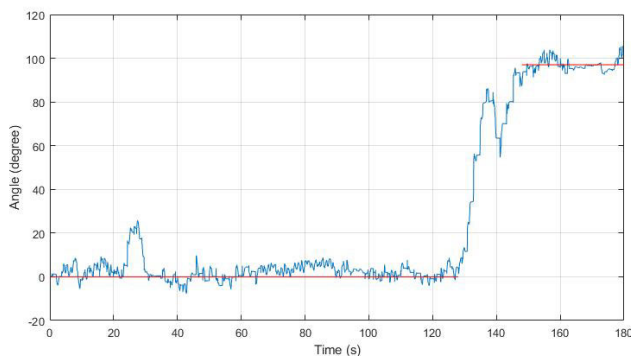
and there will exist a bias between the BLE heading and the current heading due to walking dynamics. Therefore, the replacement of heading using BLE heading will cause errors. In this article, the heading fusion is improved by correcting this bias.

Different from the fluctuation of headings, the pedestrian walking track remains straight if the heading propagates as shown in Fig. 6(a) and Fig. 6(b), and the main heading can be estimated from the line regression of previous positions. As illustrated in Fig. 8, the orientation from magnetometer and gyroscope sensors is used as the heading for PDR in the initial phase, which is influenced by magnetic disturbances, and the walking track is not precise enough to derive the main heading. When the BLE heading is estimated in the second phase, the pedestrian heading can be corrected using the BLE heading. However, a bias may exist between the BLE headings and the actual heading since the pedestrian heading fluctuates due to walking dynamics. Therefore, in the third phase, the main heading estimated from previous walking tracks during the second phase is used to correct the bias between the BLE heading and the current heading.
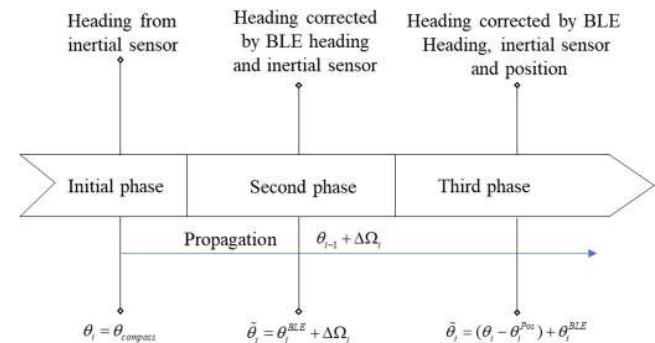

FIGURE 8. Flow chart of heading fusion using inertial sensor and BLE technique, where $\theta_{compass}$ is the compass orientation, θ^{BLE} is the BLE heading, $\Delta \Omega_i$ denotes the gyroscope integral from epoch $i - 1$ to i, and θ^{POS} is the main heading calculated from line regression of previous positions.

The high accuracy of the gyroscope integral over a short time window ensures accurate turning detection, while the update of street heading determination from the BLE technique reduces the heading error of the gyroscope integral during walking. Meanwhile, the bias correction using the main heading calculation reduces the error caused by walking dynamics. Meanwhile, once the program is started, the Bluetooth scan service will be called regularly at a certain frequency, and the iBeacon will also send Bluetooth signals continuously as long as the power is supplied. The nonstop transmission and scanning of the Bluetooth signal provide continuous heading estimation during the positioning progress. Therefore, the integration of the gyroscope and BLE can estimate the heading of pedestrians with high accuracy over a long time window.

FIGURE 7. Heading variation of pedestrians walking on the street.

H. Luo *et al.*: Integration of GNSS and BLE Technology With Inertial Sensors for Real-Time Positioning in Urban Environments

IEEE *Access*

B. POSITIONING SOLUTION OF BLE TECHNIQUE

With the use of three classes of iBeacon with different TPs, when signals from different classes of iBeacon are received, different methods are proposed to obtain positioning solutions, including calibration, weighted positioning solution and peak detection.

1) CALIBRATION SOLUTION

The weak iBeacon class is set with the lowest TP, which has the smallest coverage radius of approximately 2 m. Although its coverage is small, this class can reach an accuracy of 2 m if the signal is received. Therefore, the user position can be calibrated when a weak iBeacon class signal is received.

2) IMPROVED WEIGHTED CELL-ID SOLUTION

Since the coverage radius of the strong iBeacon class can reach 100m, the overlap of signals from different iBeacon classes can provide positioning solutions. The relationship between the RSSI value and the propagation distance represented by the path loss model [73] is expressed as

$$RSSI = RSSI_0 - 10n log_{10} d \qquad (9)$$

where $RSSI$ is the received signal strength at distance d, $RSSI_0$ is the received signal strength at the reference distance which is 1 m, and n is the mean of the path loss exponent.

n is an empirical parameter that is dependent on the local propagation environment. The collected RSSI value at 1 m, which is the reference distance, is designated as $RSSI_0$. With the known distances d and collected corresponding Bluetooth values $RSSI$, n is then fitted based on (9).

Referring to (9), the distance between the iBeacon and receiver can be computed with the RSSI measurement after the estimation of n, which is expressed as

$$d = 10^{\left(\frac{RSSI - RSSI_0}{-10n} \right)} \qquad (10)$$

The reciprocal of distance d is used as the weight for positioning. In addition, the coverage of the strong TP class is larger than that of the medium class, so the confidence in the same RSSI value from the medium class will be greater than that from the strong class. The equation of the positioning solution can be expressed as (11), shown at the bottom of the page, where W_s and W_M denote the weights of the strong and medium iBeacon classes, respectively.

To determine the weight, we conduct a field experiment. The estimated distance according to (10) is compared with the true recorded distance. For this experiment, the distance

accuracies of strong and medium TP iBeacon are 8.49 m and 6.04 m, respectively. Referring to (11), the reciprocal of distance is used as the weight to position; therefore, the weight ratio of the strong and medium iBeacon classes is finally determined as

$$\frac{W_M}{W_S} = \frac{\frac{1}{6.04}}{\frac{1}{8.49}} \approx \frac{2}{3} \qquad (12)$$

Therefore, the normalized weights of the strong and medium iBeacon classes in (11) are empirically set as 0.4 and 0.6 respectively.

3) PEAK DETECTION

Rather than the use of distance derived from the RSSI, the peak value of the RSSI is detected in this approach, and the time stamp is recorded as the time when the receiver crosses the transmitter, under the assumption that the variation of the RSSI is opposite to the variation of the distance between the receiver and transmitter in consequent motion.

To reduce the disturbances from the surroundings, the RSSI values are filtered as shown in Fig. 4. In this process, the peak point is postponed, so back searching is applied to find the maximum raw value within the time window. Afterwards, a threshold is set to compare with the maximum value and applied to judge whether the maximum is reasonable. Then, gross error detection is conducted on the consistency of the results from the medium and strong classes. Once passing the validation, the time stamp of the point when receiving the maximum value is used to correct the position.

4) POSITON CORRECTION USING BLE HEADING

If the heading contains an error $\Delta\theta$, the pedestrian position will drift with the walking distance, as shown in Fig. 9, and the distance deviating from the true position is approximately expressed as

$$\Delta D_H = d \cdot sin \Delta\theta \qquad (13)$$

where ΔD_H is the deviated distance error, d is the walking distance, and $\Delta\theta$ is the heading error.

Although the heading estimation is improved using the integration of BLE and inertial sensors, it might contain errors of several degrees due to walking dynamics. When the distance between two iBeacon is 100 meters, the position can deviate by as much as 10 meters if the heading error is 6 degrees. Therefore, a small heading error might cause a position error of up to 10 meters over a long distance. In this article, a method using BLE heading to correct the position is proposed to improve the pedestrian position precision.

$$p(E, N) = \frac{\left\{ \sum_i \left[\frac{1}{d_{S,i}} \cdot p_i(E, N) \right] \right\} \cdot W_s + \left\{ \sum_j \left[\frac{1}{d_{M,j}} \cdot p_j(E, N) \right] \right\} \cdot W_M}{\left[\sum_i \frac{1}{d_{S,i}} \right] \cdot W_s + \left[\sum_j \frac{1}{d_{M,j}} \right] \cdot W_M} \qquad (11)$$

As shown in Fig. 9, if the estimated heading contains an error $\Delta\theta$, the propagated position at epoch i will deviate from the true position. If a BLE heading is estimated at epoch i, the position will be propagated to P_j' at epoch j in our previous work [13], and the position between P_i' and P_j' will contain errors. In this article, the position at epoch i is corrected to P_i when the BLE heading is estimated to improve the position accuracy between epochs i and j as follows:

$$d = \left\| P_i' S \right\| \begin{cases} E_{p_i} = d \cdot sin\tilde{\theta} \\ N_{p_i} = d \cdot cos\tilde{\theta} \end{cases} \qquad (14)$$
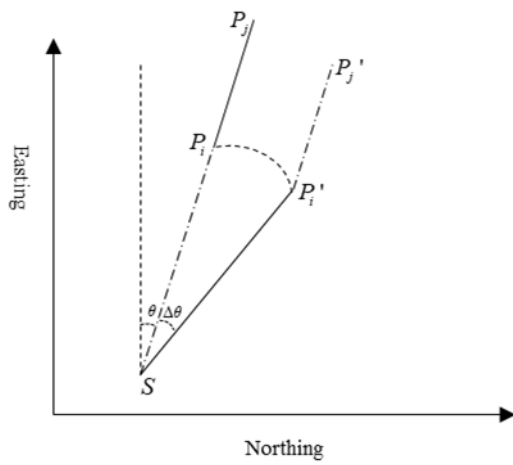

FIGURE 9. Pedestrian position drift caused by heading error.

where $P_i'S$ is the vector from S to P_i', $\tilde{\theta}$ is the corrected heading based on the proposed heading method, and E_{p_i} and N_{p_i} are the easting and northing coordinates.

C. INTEGRATION OF PDR, BLE AND GNSS

The position can be propagated with the previous location based on PDR, using the moved distance and heading, as follows:

$$\begin{cases} N_i = N_{i-1} + (1 + S_i) \cdot D_i \cdot cos\theta_i + \sigma N \\ E_i = E_{i-1} + (1 + S_i) \cdot D_i \cdot sin\theta_i + \sigma E \\ S_i = S_{i-1} + \sigma S \\ \theta_i = \theta_{i-1} + \Delta\theta_i^{gyro} + \sigma\theta \end{cases} \qquad (15)$$

where N and S denote the northing and easting coordinates of the pedestrian, subscript i is the time, S is the scale factor used to correct the distance calculated from BLE, $D = SL \cdot SN$, which is the distance calculated from step length SL and step numbers SN, θ is heading of the pedestrian, $\Delta\theta^{gyro}$ is the angular change obtained from gyroscope at time between $i - 1$ and i, and σN, σE, σS, and $\sigma\theta$ are the noise from the northing coordinate, easting coordinate, scale factor and heading, respectively.

Since the model is nonlinear, the EKF algorithm is applied, and we set the state vector as

$$X = [dN \ dE \ dS \ d\theta]^T \qquad (16)$$

where the prefix d represents the error of the four parameters.

Based on (15), the state transition model is linearized by the partial derivative, and the matrix form of this system state equation can be expressed as

$$X_i = FX_{i-1} + G\omega_{i-1} \qquad (17)$$

where X_{i-1} represents the state vector at epoch $i - 1$, F is the transition matrix, G is the system noise matrix, and ω_{i-1} is the system noise vector with the covariance matrix Q: $\omega_{i-1} \sim N(0, Q_{i-1})$.

Since the error of the four parameters in X is a small quantity, the high-order terms within linearization can be ignored, and the dynamic matrix is expressed as

$$F = \begin{bmatrix} 1 & 0 & D \cdot cos\theta & -(1 + S) \cdot D \cdot sin\theta \\ 0 & 1 & D \cdot sin\theta & (1 + S) \cdot D \cdot cos\theta \\ 0 & 0 & 1 & 0 \\ 0 & 0 & 0 & 1 \end{bmatrix} \qquad (18)$$

The measurement equation is given by

$$Z_i = H_i X_i + v_i \qquad (19)$$

where Z_i is the measurement vector, H_i is the measurement matrix, and v_i is the measurement noise with covariance matrix R: $v_i \sim N(0, R_i)$.

The positioning results from BLE and GNSS, step length correction from BLE, and heading observation from BLE are observations in this system, and the observation vector is set as

$$Z = [\Delta N \ \Delta E \ \Delta S \ \Delta\theta]^T \qquad (20)$$

The measurement matrix is given by

$$H = \begin{bmatrix} H_1 & 0 & 0 & 0 \\ 0 & H_2 & 0 & 0 \\ 0 & 0 & H_3 & 0 \\ 0 & 0 & 0 & H_4 \end{bmatrix} \qquad (21)$$

The covariance matrix is set as

$$R = \begin{bmatrix} R_1 & 0 & 0 & 0 \\ 0 & R_2 & 0 & 0 \\ 0 & 0 & R_3 & 0 \\ 0 & 0 & 0 & R_4 \end{bmatrix} \qquad (22)$$

Due to the uncertainty of the reception of GNSS and BLE signals, the parameters in Z, H, and R are set based on the observations.

(1) If the positioning solution from BLE is updated, the parameters in Z are set as

$$\begin{cases} \Delta N = N_{iBeacon} - N_{PDR} \\ \Delta E = E_{iBeacon} - E_{PDR} \end{cases} \qquad (23)$$

The parameters in H are set as

$$H_1 = H_2 = 1 \qquad (24)$$

H. Luo *et al.*: Integration of GNSS and BLE Technology With Inertial Sensors for Real-Time Positioning in Urban Environments

IEEE *Access*

The parameters in R are set as

$$\begin{cases} R_1 = \sigma_{iBeacon\_N}^2 \\ R_2 = \sigma_{iBeacon\_E}^2 \end{cases} \tag{25}$$

where $\sigma_{iBeacon\_N}$ and $\sigma_{iBeacon\_E}$ are determined based on the distance between the user and the iBeacon, which is calculated by the RSSI referring to (10) and expressed as

$$d_{iBeacon} = f(RSSI) \begin{cases} \sigma_{iBeacon\_N} = d_{iBeacon} \cdot cos\theta \\ \sigma_{iBeacon\_E} = d_{iBeacon} \cdot sin\theta \end{cases} \tag{26}$$

(2) If the positioning solution from GNSS is updated, the parameters in Z are set as

$$\begin{cases} \Delta N = N_{GNSS} - N_{PDR} \\ \Delta E = E_{GNSS} - E_{PDR} \end{cases} \tag{27}$$

The parameters in H are set as

$$H_1 = H_2 = 1 \tag{28}$$

The parameters in R are set as

$$R_1 = R_2 = \sigma_{GNSS}^2 \tag{29}$$

The σ_{GNSS} is calculated as follows steps:

(a) The GNSS output quality is evaluated using two thresholds, including the horizontal dilution of precision (HDOP) and precision from the raw output. The thresholds are preset to evaluate the quality of the GNSS measurements.

(b) For those epochs where the GNSS results meet the demands of quality evaluation, the difference between the GNSS and PDR movements in those epochs is calculated.

$$\begin{cases} \Delta dis_i^{GNSS} = norm\left(Pos_i^{GNSS} - Pos_{i-1}^{GNSS}\right) \\ \Delta dis_i^{PDR} = norm\left(Pos_i^{PDR} - Pos_{i-1}^{PDR}\right) \end{cases} \tag{30}$$

where Pos_i^{GNSS} and Pos_i^{PDR} are the GNSS and PDR positioning results in epoch i respectively.

(c) When the length of effective epochs is larger than the preset threshold, the difference within these epochs is applied to determine the GNSS noise matrix, which is expressed as

$$\sigma_{GNSS} = \sqrt{\frac{\Delta^T \Delta}{m}} \tag{31}$$

$$\Delta = \sum_{i=1}^{I} \Delta dis_i^{GNSS} - \sum_{i=1}^{I} \Delta dis_i^{PDR} \tag{32}$$

where i indicates those epochs in which the GNSS results meet the demands of quality evaluation, and Δ indicates the difference between the GNSS and PDR in those epochs. m expresses the number of the epochs.

(3) If the step length correction from BLE is updated, the corresponding parameter is set as: $\Delta S = \Delta S^{BLE}$, $H_3 = 1$, and $R_3 = 0.01^2$.

(4) If the heading from BLE is updated, the corresponding parameter is set as $\Delta \theta = \theta^{BLE} - \theta^{PDR}$, $H_4 = 1$, and $R_4 = 0.01^2$.

The construction of the measurement matrix is then based on the combination of the four cases corresponding to the received measurements. If position, scale factor or heading is not observed, the corresponding parameters are set as 0 in H.

Then, the coordinates of the pedestrian can be updated by the following equation:

$$\begin{cases} N_i = N_{i-1} + dN_{i-1} + (1 + S_{i-1} + dS_i) \cdot D_{i-1} \\ \quad \cdot cos\left(\theta_{i-1} + d\theta_i\right) \\ E_i = E_{i-1} + dE_{i-1} + (1 + S_{i-1} + dS_i) \cdot D_{i-1} \\ \quad \cdot sin\left(\theta_{i-1} + d\theta_i\right) \end{cases} \tag{33}$$

As mentioned above, the traditional KF is unsuitable in nonlinear systems, while the EKF and UKF have been proposed for nonlinear dynamic systems. For general state-space problems, the computational complexity of the EKF and UKF equals $O\left(L^3\right)$, where L is the dimension of the state parameter [74]. However, the estimation process of the EKF is easier than UKF that the EKF is more computationally efficient [66]. Compared with the KF-based approach, the STKF increases the calculation of the fading factor, whose computational expense is not augmented [63], and its computational complexity also equals $O\left(L^3\right)$ in the same case. For the FF, the computational complexity is $O\left(N^3 + \sum M \times N^2\right)$, where N is the number of filter states and M is the total number of measurements of all sensors. With the increase in the number of sensors, the computational complexity grows significantly [75]. The computational complexity of a PF is $O\left(PL^2\right)$, where P is the number of particles. Its calculation demand is P/L times the EKF, which means that the number of particles must be increased to achieve a more accurate estimation. Therefore, P is much larger than L, and the computational complexity of a PF is much larger than that of an EKF.

Among the above filters, the low computational complexity of the EKF guarantees real-time implementation on smartphones.

III. EXPERIMENTAL SET UP AND RESULTS
As mentioned above, step detection, step length and heading estimation are key elements in PDR, and absolute positioning solutions for correction are also an important part of integration. The performance of the three elements in PDR and positioning solutions from the BLE technique were assessed with several experiments. Then, several field experiments were conducted to evaluate the performance of the integration system in different environments. In all experiments, the sampling frequencies (SFs) of the accelerometer and magnetometer were set as 50 Hz, and the SF of the gyroscope was set as 100 Hz, the SF of the GNSS was 1 Hz, and the broadcast interval of the iBeacon was 100ms.

A. STEP DETECTION EVALUATION
After the implementation of the pedometer on Android-based smartphones, several experiments were conducted to evaluate

IEEE *Access*

H. Luo *et al.*: Integration of GNSS and BLE Technology With Inertial Sensors for Real-Time Positioning in Urban Environments

the proposed approach considering different devices, walking speeds and users. In the first experiment, an experimenter walked at three speeds- normal, slow, and fast- holding two devices simultaneously. The statistical results are shown in Table 2.

TABLE 2. Accuracy of the pedometer with different speeds and devices.

Speed	HUAWEI Mate9		HUAWEI P10	
	Error (%)	Max error (%)	Error (%)	Max error (%)
Normal	0.5	0.6	0.5	1.2
Slow	0.7	1.2	0.7	1.2
Fast	1.0	2.0	0.7	1.9

The test results showed that the pedometer can estimate steps with high accuracy, despite the user's walking speed. The averaged error was below 1.0%, and the maximum error was 2.0% at the fast speed. Moreover, the experimental results from different types of smartphones showed that this algorithm performs well in different Android-based phones. Therefore, the pedometer was able to detect steps with high accuracy regardless of different devices and different user walking speeds.

The pedometer was also tested for different users at normal speeds. Eight experimenters, including males and females, were involved in evaluating the step detection algorithm for individuals, and the results are listed in Appendix I.

From the results, it can be seen that the pedometer had a high accuracy in detecting steps among different users, where the maximum error was 1% and the averaged error was below 0.5%. The results indicated that the pedometer had a high accuracy and was applicable for different users.

To evaluate the performance of step detection under unconstrained conditions, several experiments were conducted, and four experimenters were involved, including males and females, putting smartphones in eight positions, and the total step count for each experiment was 200. The statistical results of all experiments are listed in Table 3, and detailed step counts and errors for each test using the proposed approach and previous method [13] are shown in Appendix II.

The experimental results showed that step detection in the time domain failed to count steps accurately when the smartphones were held in swing hands or placed in trouser pockets, backpacks and chest pockets with an average error of the eight activities at approximately 15.5% and a maximum error of 50.5% in swing hand activity. Specifically, if smartphones are prone to shaking or over movements, the accuracy of the previous method [13] was poor. Meanwhile, the previous step detection failed to count approximately half of the total steps when the smartphones were held in the swing hand, since the method detected swing motion as walking, and the frequency of swinging was approximately about half of the walking frequency. By contrast, step detection using the proposed method could count steps more accurately under different conditions, and the average error was approximately 1.0%,

TABLE 3. Accuracy of pedometer with different postures.

Test ID	Activity	Step detection with FFT		Step detection in time domain	
		Error (%)	Max error (%)	Error (%)	Max error (%)
1	Holding	0.6	1.5	1.1	2.0
2	Phoning	1.3	2.0	1.7	3.3
3	Swing hand	2.2	5.5	48.7	50.5
4	Trouser front pocket	0.9	3.5	21.9	48.3
5	Trouser back pocket	0.8	2.8	27.4	45.3
6	Backpack	0.8	2.0	7.6	25.8
7	Handbag	1.0	2.8	4.5	19.3
8	Chest pockets	0.7	1.5	11.1	42.5

whereas the maximum error was 5.5%, compared to the maximum error of 50.5% from the previous method. In most cases, the proposed method could detect steps with an error lower than 2%. In swing hand activity, the acceleration magnitude of swing motion was larger than the acceleration caused by walking, and the frequency filter have been affected, resulting in a larger error of approximately 5%.

In conclusion, the proposed method is more robust for different types of activities than time domain-related methods, and the proposed method exhibits a better performance, with an average error of approximately 1.0%. The error of step detection when smartphones are held in the swing hand can be reduced from $\sim 50\%$ to 5%. Therefore, the proposed method can be employed to detect steps when smartphones are held under unconstrained conditions with high accuracy.

B. STEP LENGTH ESTIMATION EVALUATION

As mentioned above, several step length estimation models have been proposed. The empirical linear model is more applicable since no training phase is required. In this article, several experiments were conducted to compare the linear model with other popular models to evaluate their accuracy on step length estimation. In the step length evaluation experiments, two experimenters were involved, and two devices were used. For each experimenter, 25 tests were conducted for each smartphone, so a total of 100 tests were conducted. In each experiment, the true total length was 50 meters, and the total length estimated from the three models was calculated with the following equation, expressed as

$$TL = \sum SL \cdot SF \tag{34}$$

where TL is the total length, which equals 50 m in all experiments, SL is the step length of each step, and SF is the step frequency estimated from step detection.

The difference between the true and obtained total lengths were considered the error of step length estimation. The statistical results are shown in Table 4.

By comparing the error of the total length of the estimated step length using three models, the results shown

H. Luo *et al.*: Integration of GNSS and BLE Technology With Inertial Sensors for Real-Time Positioning in Urban Environments

IEEE *Access*

Tᵃ	Mᵇ	HUAWEI P10				HUAWEI Mate9			
		Mxᶜ (m)	Sᵈ (m)	Mx (%)	S (%)	Mx (m)	S (m)	Mx (%)	S (%)
1	A	3.8	2.4	7.5	4.7	3.4	2.3	6.8	4.6
	B	3.4	1.8	6.7	3.6	2.5	1.2	5.0	2.4
	C	1.9	0.8	3.9	1.6	1.7	0.7	3.4	1.4
2	A	3.9	1.8	7.9	3.5	4.3	1.7	8.6	3.4
	B	4.7	1.9	9.4	3.8	4.5	1.7	9.0	3.4
	C	1.9	0.8	3.7	1.7	1.9	1.0	3.8	2.0

ᵃT represents the ID of the experiments; ᵇM indicates the applied models, where A, B and C are constant, nonlinear and linear models, respectively; ᶜMx represents the maximum error in the experiment; and ᵈS indicates the standard deviation of the error in the experiment.

in Table 4 show that the linear model has a higher accuracy than the other applied models, with a maximum error of 1.9 meters and the standard deviation (STD) is under one meter in a total length of 50 meters. Here, the linear model was applied in this system. In the initial phase, the parameter c in the linear model was set as one. In the online phase, the parameter c was corrected with the help of BLE technology to estimate a better step length.

C. COMPARISON OF HEADING ESTIMATION FROM DIFFERENT APPROACHES

The conventional sensors used to obtain headings in PDR are gyroscopes and digital compasses, whereas a heading estimation method based on BLE and inertial sensors is proposed here. To evaluate their performances, two experiments were conducted in different environments to compare the headings obtained from the proposed BLE-based approach, digital compass and gyroscope (given the known heading for the gyroscope in the first epoch). The lane or street heading was regarded as the reference "true" heading. Specifically, considering the walking dynamics of the pedestrian, the actual heading of the pedestrian would swing up and down around the reference street direction. Fig. 10 and Fig. 11 show the comparisons of headings from the compass, the gyroscope and the hybrid approach of BLE and an inertial sensor. In addition, Table 5 shows the comparisons of the heading estimation accuracy among the three methods.

TABLE 5. Comparison of accuracy of heading estimation in two experiments.

Methods	Experiment 1 (Short distance)		Experiment 2 (Long distance)	
	Mean (degree)	STD (degree)	Mean (degree)	STD (degree)
Compass heading	5.8	17.4	6.3	12.9
Gyroscope integral	-5	9	-25.1	21.9
Fused method	3.4	9.3	-3	9.2

In Fig. 10, the experimental results show that headings from compass reading fluctuated more among the three types of techniques and methods, and the compass was influenced by undesired magnetic effects, resulting in large heading errors between 120 s and 140 s, whereas the error of heading estimated from the compass reached approximately
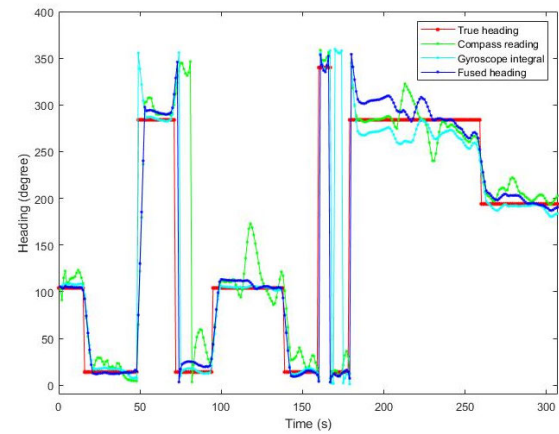
FIGURE 10. Heading comparison of different methods in the first experiment results between true heading, compass reading, gyroscope integral and fused heading.
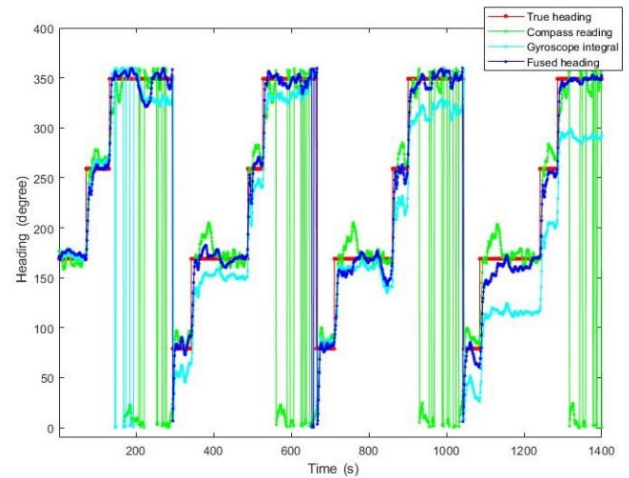
FIGURE 11. Heading comparison of different methods in the second experiment results between true heading, compass reading, gyroscope integral and fused heading.

70 degrees. As seen from the result at approximately 70 s shown in Fig. 10, the turning detection from the gyroscope and the fused method was more sensitive to turning than that from the compass. In a short time window, the gyroscope integral showed good performance in heading estimation when the true initial heading was given. The heading estimation using the fused method showed consistency with the gyroscope integral without the known initial heading.

The duration of the second experiment was approximately 5 times the duration of the first experiment, as shown in Fig. 11, and the results showed that the error of the gyroscope integral increased with time. During a long time window, the error of heading estimation from the gyroscope integral reached 90 degrees. Similar to the first experiment, the headings estimated from the compass contained more noise. The heading estimation using the fused method performed well with a high accuracy throughout the second experiment.

As shown in Table 5, with the help of integrating BLE technology and gyroscope, the heading estimation achieved

IEEE Access

H. Luo et al.: Integration of GNSS and BLE Technology With Inertial Sensors for Real-Time Positioning in Urban Environments

a mean error of approximately 3 degrees in the two experiments, and the STD of the errors was approximately 9 degrees in the two experiments due to the walking dynamics of pedestrians as mentioned above. By contrast, the errors of heading estimated from the compass were larger than those from the fused method in the two experiments, at 5.8 degrees and 6.3 degrees, respectively, with higher STDs of error at 17.4 degrees and 12.9 degrees, respectively. During a short time window, the mean error from the gyroscope integral reached −5.0 degrees, but it degraded to −25.1 degrees over a long duration with a higher STD of heading error.

In the two experiments, the readings from the digital compass contained large errors when the compass was influenced by the magnetic effects of the surroundings. Compared with gyroscope values, the readings from the compass fluctuated more. On the other hand, the gyroscope sensors could detect pedestrian turning rapidly with high accuracy, and the error from the gyroscope was small in a short term. However, the gyroscope error after a long-term accumulation could reach 90 degrees if there was no external correction. In the two experiments, the fused approach could obtain headings with better performance compared with the compass or gyroscope alone. The results using the proposed method were more accurate, robust, and sensitive to turning.

D. EVALUATION OF BLUETOOTH LOW ENERGY POSITIONING

An experiment was conducted to evaluate the positioning accuracy using the calibration method, improved weighted cell-ID solution, and peak detection, and the detailed accuracy is shown in Table 6.

The results showed that the calibration approach could achieve high accuracy (0.3 m) positioning in an urban environment if a signal was received, whereas its availability was lower than 4%. In the improved weighted cell-ID, the combination of medium and strong iBeacon classes improved the availability and accuracy compared with the single class. Moreover, the peak detection on the medium and strong classes could achieve high accuracy at 8.3 m and 9.4 m, respectively, and the gross exclusion based on the combination of two classes could improve the accuracy to 5.6 m, with the lowest availability below 1%, as shown in Fig. 12.

In conclusion, the calibration and peak detection approaches can provide high precision, but their availability is low, whereas the weighted cell-ID approach can provide more positioning solutions with relatively lower accuracy. The weighted cell-ID method can be used in the initial stage to provide rough position and accurate street information to assist the GNSS-based approaches.

E. POSITIONING RESULTS IN FIELD EXPERIMENTS

To evaluate the performance of this integration system, an experiment was conducted in typically highly urbanized areas (Mong Kok in Hong Kong). Then, repeated experiments were conducted in the same area to validate the

TABLE 6. Positioning accuracy and availability using the BLE technology.

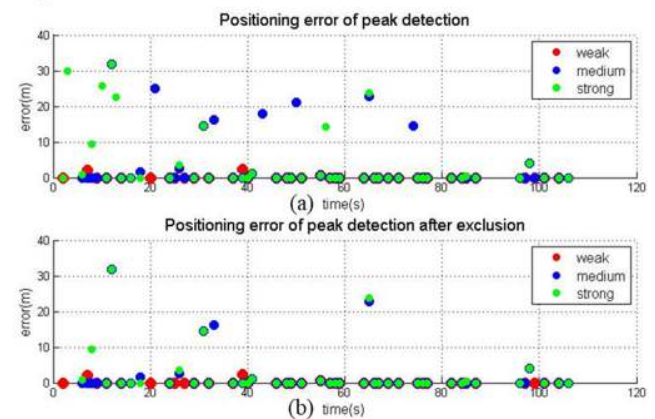| Method	iBeacon class	Availability (%)	Error (m)
Calibration	Weak	3.8	0.3
Improved weighted cell-ID	Medium	15.0	15.2
	Strong	46.0	20.0
	Medium & strong	50.3	15.9
Peak detection	Medium	0.8	8.3
	Strong	0.8	9.4
	Medium & strong	0.7	5.6

FIGURE 12. Positioning error of peak detection approach.

improvement of this system. Finally, an experiment was carried out in a more complex environment that contained indoor and outdoor areas to validate its performance with unconstrained smartphones.

The first two experiments were conducted in a typical deeply urbanized area, as shown in Fig. 13(a), where the cyan line indicates the walking route. Fig. 13(b) shows the surroundings of the experiments, in which the streets are narrow and surrounded by tall buildings. Groups of iBeacon devices were installed on lampposts since the coordinates of
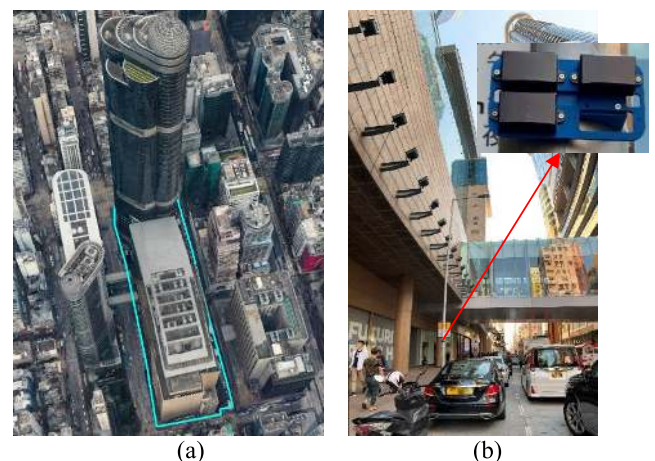

(a)   (b)

FIGURE 13. Experimental setup illustrations. (a) Illustration of the experimental site; (b) Illustration of the real environment of experimental site and one group of iBeacon installed on a lamppost.

H. Luo *et al.*: Integration of GNSS and BLE Technology With Inertial Sensors for Real-Time Positioning in Urban Environments

IEEE *Access*

all lampposts in Hong Kong are available from the website of the Land Department of Hong Kong. On each lamppost, three iBeacon classes- weak, medium, and strong class- were installed at the same height, at approximately 1.8 m, as shown in Fig. 13(b).

The size of the experimental region was approximately $185 \times 60 m^2$, in which 12 groups of iBeacon were installed on lampposts, and the intervals between two neighboring groups of iBeacon varied from 30 m to 80 m depending on the lamppost locations. As shown in Fig. 14, the purple dots indicate the location of the lamppost where groups of iBeacon were installed; the red line shows the route track of the experiment, with the starting point indicated with a blue triangle, and the black arrows indicate the moving heading of the user. In these experiments, the ground truth was generated using interpolation between two known coordinates of the lamppost with estimated steps from our method mentioned above, which showed an error ratio below 1%.

FIGURE 14. Demonstration of the ground truth and lamppost position installed with iBeacon on the developed system.

1) EVALUATION OF INTEGRATION SYSTEM

The integration system includes real-time and postprocess modes with an update frequency of 50 Hz. The synchronization of data from different sources is based on the time stamp of each variable. In real-time mode, the positioning results are shown on the smartphones as shown in Fig. 15(d), with the ground truth supplemented after the experiment for comparison. Simultaneously, all data, including inertial sensor data, raw GNSS data and raw BLE data, were recorded for postprocessing. To evaluate the performance of different technologies in the system, three modes were analyzed during postprocessing, including GNSS-only, GNSS and PDR integration, and the integration of GNSS, PDR, and BLE position

(a) (b) (c) (d)
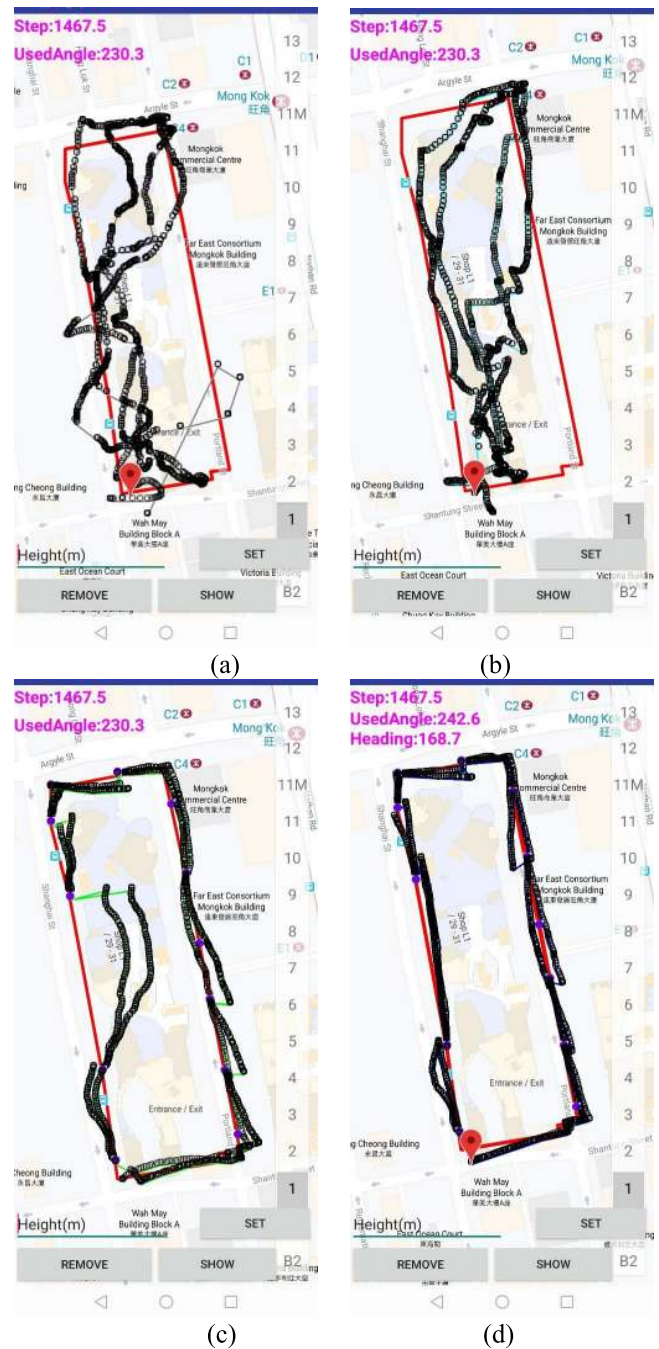
FIGURE 15. Positioning results of the technology integration. (a) GNSS only; (b) Integration of GNSS and PDR technology; (c) Integration of GNSS, PDR, and BLE technology, where BLE technology provides positioning results only; (d) Integration of GNSS, PDR, and BLE technology, where BLE technology provides positioning results and heading corrections.

correction, and the results are shown in Fig. 15(a), (b), and (c), respectively. In Fig. 15, each black dot shows the positioning results in each epoch, connected by the colored line in the time sequence, and the red line represents the ground truth. The positioning accuracy statistics are shown in Table 7.

As shown in Fig. 15(a), GNSS-only positioning results contained large errors with the horizontal accuracy in excess of 30 meters, which was mainly caused by severe multipath

IEEE *Access*

H. Luo *et al.*: Integration of GNSS and BLE Technology With Inertial Sensors for Real-Time Positioning in Urban Environments

TABLE 7. Positioning accuracy of four methods.

Methods	STD(m)		
	Northing	Easting	Horizontal
GNSS-only	11.2	28.1	30.2
GNSS+PDR	11.3	22.1	24.8
GNSS+PDR+BLE (position only)	2.1	7.9	8.1
GNSS+PDR+BLE (position + heading)	2.9	3.0	4.2

and NLOS effects. After integration with PDR, the outliers in the GNSS positioning results were filtered out with the results shown in Fig. 15(b), and the accuracy improved to 24.8 m. Then, the conventional integration method using the GNSS, PDR, and BLE techniques was tested, as shown in Fig. 15(c). The positioning results were obviously more accurate, and the horizontal accuracy improved to 8.1 m. These results further provide good evidence of the great potential of BLE in outdoor positioning. However, the large errors in heading estimation cannot be ignored as shown on the left side of the experimental region in Fig. 15(c). To overcome this problem, the new heading estimation method based on the BLE technique was applied in our system. As shown in Fig. 15(d), the estimated headings were more accurate than those in Fig. 15(c), which further improved the accuracy of positioning solutions from 8.1 m to 4.2 m.

From the above experimental results, the integration of the GNSS, PDR, and BLE (providing positioning solution and heading estimation) achieved the best positioning accuracy of 4.1 m, which validates the performance of our integration system in a highly urbanized environment. Ji *et al.* showed that when more beacons are engaged, the positioning results are more accurate. To achieve a positioning accuracy of 5 m, the beacon intervals must be less than 5 m [76]. With our algorithm, the same level of accuracy was achieved with iBeacon interval ranges of up to 150 m, as demonstrated in the experiment; hence, the installation cost can be significantly reduced.

2) EVALUATION OF THE IMPROVEMENT OF THE INTEGRATED SYSTEM

To further validate the performance of the new integration system in an urban environment, and assess the improvement over the previous system [13], two experiments were carried out in the same areas as the previous experiments. Figs. 16 and 17 show the results of the two experiments, where the left and right figures represent the positioning results using the previous system and our improved system, respectively, and the statistics of the positioning accuracy are listed in Tables 8 and 9, respectively.

In the first test shown in Fig.16, the availability rate of heading estimation was improved based on the current heading turning detection (seen in green rectangles A and B), since the RSSI list received in previous epochs would remain for BLE heading estimation in the current system, whereas it was cleared in the previous system when a turn occurred, as shown in Fig. 6(b). Then, the heading accuracy was also improved
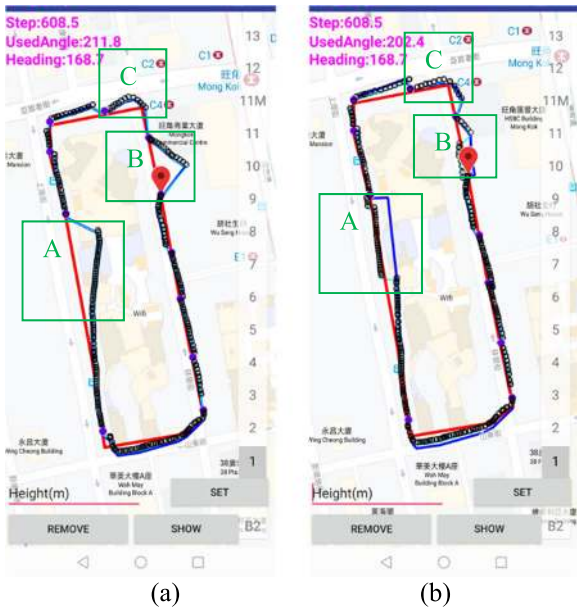
FIGURE 16. Comparison of positioning results using two systems in the first experiment. (a) Integrated positioning results using the previous system; (b) Integrated positioning results using the improved system.
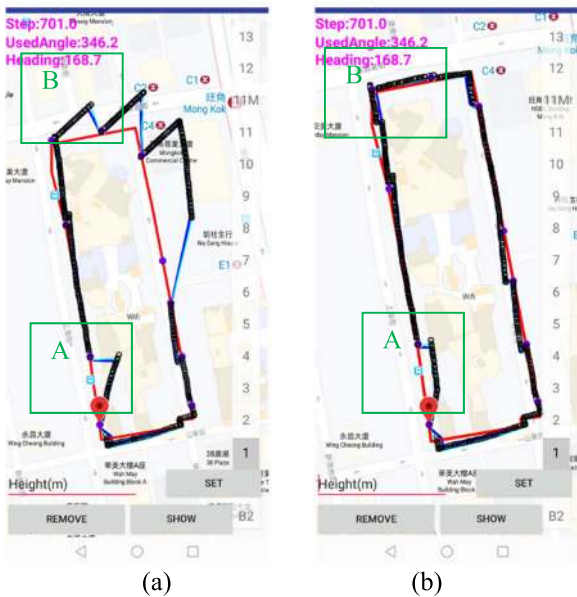
FIGURE 17. Comparison of positioning results in the second experiment using two systems. (a) Integrated positioning results using the previous system; (b) Integrated positioning results using the improved system.

TABLE 8. Positioning accuracy of previous and improved system.

System	RMS(m)		
	Northing	Easting	Horizontal
Previous	3.9	5.4	6.7
Improved	2.3	2.1	3.1

based on the improvement of heading fusion, shown in green rectangle C. In addition, the proposed position correction

H. Luo *et al.*: Integration of GNSS and BLE Technology With Inertial Sensors for Real-Time Positioning in Urban Environments

IEEE *Access*

TABLE 9. Positioning accuracy of previous and improved system.

System	RMS(m)		
	Northing	Easting	Horizontal
Previous	26.0	7.8	27.2
Improved	1.8	2.0	2.7

TABLE 10. Positioning availability and accuracy.

Methods	Availability (%)	RMS(m)		
		Easting	Northing	Horizontal
GNSS	50.8	23.1	7.0	24.7
PDR+BLE+GNSS	100.0	1.8	1.6	2.4

using BLE heading could also largely improve the accuracy of pedestrian position, especially in the long distance between two base stations or large heading correction, seen in green rectangles A and B. The statistics show that the positioning accuracy was improved from 6.7 m to 3.1 m in northing and easting, respectively.

In the second test shown in Fig. 17, the new heading estimation method also performed well as marked with green rectangles A and B, which largely improved the heading accuracy in the propagation progress, and the accuracy of the positioning results showed a large improvement from 27.2 m to 2.7 m.

From the experimental results, it can be seen that the heading estimation using our methods was more robust than the previous estimation. The positioning results of the improved system were more consistent with the true route while its positioning accuracy achieved ∼3 m. It is mainly based on the improvement of heading estimation and the position correction.

3) EVALUATION OF THE IMPROVED INTEGRATION SYSTEM WITH AN UNCONSTRIANED SMARTPHONE

Finally, to evaluate the feasibility of the integration system in a more complex but common scenario, an experiment was conducted in an environment containing indoor and outdoor areas. In addition, the performance of the system with unconstrained smartphones was also validated to provide a basis for further application in highly urban environments. The experimental setup is shown in Fig. 18, including indoor and outdoor areas.

In indoor areas, PDR and BLE play vital roles in providing positions, whereas the GNSS is unavailable in this situation. In the outdoor environment, the system estimates the pedestrian positions based on the integration of the GNSS, PDR, and BLE techniques. The positioning results using the GNSS only and the integration system are shown in Fig. 18(a) and Fig. 18(b), respectively, and the statistics of availability and positioning accuracy are shown in Table 9.

In Fig. 19, it can be seen that the integration system could provide a stable positioning solution with high

FIGURE 18. Environment and pedestrian route of the experiment in indoor and outdoor environments.

FIGURE 19. The positioning results with unconstrained smartphones in indoor and outdoor areas: (a) Positioning results of raw GNSS; (b) Positioning results using integration system of GNSS, PDR, and BLE techniques.

accuracy in indoor areas. In outdoor areas, the integration system largely improved the positioning accuracy of 2.4 m, compared to the accuracy of GNSS positioning at approximately 25 m. In addition, the availability of positioning was highly improved. Corresponding to the accuracy improvement compared to the outdoor experiment on streets, this is mainly because of the higher density of iBeacon installations. In addition, the positioning accuracy with unconstrained smartphones can reach a few meters owing to the high accuracy and stability of our step detection method.

IEEE *Access*

H. Luo *et al.*: Integration of GNSS and BLE Technology With Inertial Sensors for Real-Time Positioning in Urban Environments

TABLE 11. Accuracy of the pedometer for different experimenters.

Test ID	ID[a]	True (step)	Pedometer (step)	Error (step)	Accuracy (%)
1	A	220	220	0	0.0
2		218	217.5	-0.5	0.2
3	B	221	220	-1	0.5
4		222	223	1	0.5
5	C	238	238	0	0.0
6		235	233	-2	0.9
7	D	230	230	0	0.0
8		230	229	-1	0.4
9	E	200	201	1	0.5
10		200	200.5	0.5	0.3
11	F	200	200.5	0.5	0.3
12		200	199.5	-0.5	0.3
13	G	200	200	0	0.0
14		200	199	-1	0.5
15	H	200	198	-2	1.0
16		200	200.5	0.5	0.3

[a]ID represents the ID of the experimenters.

The experimental results validate the feasibility of the integration system in this more complex scenario, which is common in urban cities. This further provides an opportunity to solve the seamless positioning problem for urban environments.

IV. CONCLUSION AND FUTURE WORKS

In deep urban canyons, the performance of conventional GNSS positioning can be easily affected by the blockage and reflection of GNSS signals. The integration of the GNSS and PDR techniques shows obvious improvements in positioning availability and accuracy, depending on continuous updates of absolute positioning with high accuracy. BLE technology, which is usually applied in indoor positioning, shows great potential in outdoor positioning. The EKF guarantees the real-time performance of the algorithm implementation on smartphones with its low computational complexity. In our previous work, an integration system of the GNSS, PDR, and BLE techniques in smartphones was proposed and primarily verified in deep urban canyons, however its accuracy was not fully evaluated, and the performance also required further investigation. In this work, we proposed several methods to improve the accuracy of each component of the PDR algorithm, including step detection, heading estimation, and absolute position, to further improve the performance of the whole integration system.

Several experiments were carried out to evaluate the accuracy of each method, and then the performance of the integration system was assessed through field experiments in different environments. First, the step detection method performed well, with errors below 1% among different walking speeds and users. Especially for different pedestrian activities, the mean error ratio in the eight tested situations was reduced from 15.5% to 1.0%, which further validates that our method is more robust than time-domain-based methods under unconstrained conditions. Second, the heading estimation combining the BLE technique and inertial sensors was integrated into this system, and turning detection and

TABLE 12. Accuracy of the pedometer for different experimenters in different activities.

Tester ID	Activity	Step detection with FFT		Step detection in time domain	
		Count steps	Error (%)	Count step	Error (%)
1	Holding	199.5	-0.3	202.0	1.0
		197.5	-1.3	200.5	0.3
	Phoning	197.5	-1.3	196.5	-1.8
		198	-1.0	200.0	0.0
	Swing hand	190	-5.0	102.0	-49.0
		192	-4.0	101.5	-49.3
	Trouser front pocket	200	0.0	200.0	0.0
		199	-0.5	202.0	1.0
	Trouser back pocket	199	-0.5	270.0	35.0
		201	0.5	273.5	36.8
	Backpack	199	-0.5	196.5	-1.8
		199.5	-0.3	202.0	1.0
	Handbag	199	-0.5	203.5	1.8
		200.5	0.3	203.5	1.8
	Chest	199.5	-0.3	201.5	0.8
		200.5	0.3	202.5	1.3
2	Holding	200.5	0.3	202.5	1.3
		199.5	-0.3	200.5	0.3
	Phoning	196	-2.0	200.5	0.3
		199	-0.5	200.5	0.3
	Swing hand	199	-0.5	101.5	-49.3
		199	-0.5	104.0	-48.0
	Trouser front pocket	199.5	-0.3	279.5	39.8
		201.5	0.8	285.0	42.5
	Trouser back pocket	199	-0.5	213.0	6.5
		201	0.5	216.0	8.0
	Backpack	202	1.0	203.5	1.8
		200	0.0	205.5	2.8
	Handbag	199.5	-0.3	204.0	2.0
		200	0.0	200.0	0.0
	Chest	199	-0.5	203	1.5
		197	-1.5	201	0.5
3	Holding	200.5	0.3	202.0	1.0
		200	0.0	204.0	2.0
	Phoning	199	-0.5	206.0	3.0
		196	-2.0	206.5	3.3
	Swing hand	202	1.0	104.0	-48.0
		201	0.5	104.5	-47.8
	Trouser front pocket	198	-1.0	205.5	2.8
		198	-1.0	202.0	1.0
	Trouser back pocket	199	-0.5	238.5	19.3
		198.5	-0.8	264.0	32.0

H. Luo *et al.*: Integration of GNSS and BLE Technology With Inertial Sensors for Real-Time Positioning in Urban Environments

IEEE *Access*

TABLE 12. *(Continued.)* Accuracy of the pedometer for different experimenters in different activities.

	Backpack	200	0.0	216.5	8.3
		196	-2.0	222.0	11.0
	Handbag	197	-1.5	212.5	6.3
		201	0.5	208.0	4.0
	Chest	199.5	-0.3	285	42.5
		198.5	-0.8	244	22.0
	Holding	198.5	-0.8	202.0	1.0
		197	-1.5	203.5	1.8
	Phoning	196	-2.0	205.5	2.8
		198	-1.0	204.0	2.0
	Swing hand	201	0.5	105.0	-47.5
		189	-5.5	99.0	-50.5
4	Trouser front pocket	207	3.5	296.5	48.3
		199	-0.5	280.5	40.3
	Trouser back pocket	199.5	-0.3	290.5	45.3
		194.5	-2.8	273.0	36.5
	Backpack	196.5	-1.8	217.5	8.8
		202	1.0	251.5	25.8
	Handbag	194.5	-2.8	198.0	-1.0
		196	-2.0	238.5	19.3
	Chest	197.5	-1.3	216.5	8.3
		198.5	-0.8	223.5	11.8

heading fusion were improved in this article. The accuracy of the heading estimation method achieved a mean error of approximately 3 degrees in the two experiments, which is superior to the digital compass and gyroscope-only method. The proposed method provides a more reliable heading estimation method than other common methods since it is free from the magnetic interference of surroundings and can obtain absolute headings with high accuracy. Third, based on the novation of BLE application on heading estimation, the same level of positioning accuracy can be achieved with fewer iBeacon installations, thus reducing expense. The new positioning method based on the BLE technique can achieve accuracies of 0.3 m and 5.6 m by employing the calibration and peak detection approaches, respectively, whereas the weighted cell-ID approach can provide a positioning solution to assist the GNSS at the initial phase.

Finally, large positioning errors were filtered out by integrating of the GNSS and PDR, and the positioning accuracy was improved to 24.8 m, compared to 30.2 m from the GNSS alone. After the integration of BLE positioning, the accuracy was improved to 8.1 m. Using the previous method of BLE heading, the positioning accuracy could reach 6.7 m, however, the heading estimation algorithm was unstable. This degraded the positioning accuracy to 27.2 m in repeated experiments. Based on the improvement of heading estimation and position correction with BLE heading, the positioning accuracy of the improved integration system achieved

2.7 m and 4.2 m in repeated experiments. Compared to other common methods, including compass-based methods, gyroscope integration, and our previous approach based on the BLE and gyroscope, the current method is more robust in estimating headings for pedestrians. Moreover, the experimental results validate the feasibility of the integration system in seamless environments, and the positioning accuracy with unconstrained smartphones can reach a few meters owing to the high accuracy and stability of our step detection method.

Our integration system was implemented under the installation of BLE sensors in typical regions of Hong Kong, and it mainly provided pedestrian positioning in those urban regions. With the construction of smart cities, more information will be available, such as BLE and other types of transmitter networks, road database sources and 3D building maps in Hong Kong. This will provide opportunities for systems to assist in GNSS positioning. In the future, we will focus on the integration of the current system with a map-based method to obtain more robust positioning solutions in pedestrian navigation, thus increasing the availability in more areas.

APPENDIX
See Tables 11 and 12.

REFERENCES

[1] M. Weinlich, P. Kurz, M. B. Blau, F. Walcher, and S. Piatek, "Significant acceleration of emergency response using smartphone geolocation data and a worldwide emergency call support system," *PLoS ONE*, vol. 13, no. 5, May 2018, Art. no. e0196336.

[2] M. Adjrad, P. D. Groves, J. C. Quick, and C. Ellul, "Performance assessment of 3D-mapping-aided GNSS—Part 2: Environment and mapping," *Navigation*, vol. 66, no. 2, pp. 363–383, Jun. 2019.

[3] B. Ricker and R. E. Roth, "Mobile maps and responsive design," *Geographic Inf. Sci. Technol. Body Knowl.*, vol. 2018, no. Q2, p. 40, Apr. 2018.

[4] Y. Li, Y. Zhuang, H. Lan, P. Zhang, X. Niu, and N. El-Sheimy, "Self-contained indoor pedestrian navigation using smartphone sensors and magnetic features," *IEEE Sensors J.*, vol. 16, no. 19, pp. 7173–7182, Oct. 2016.

[5] L.-T. Hsu, "Analysis and modeling GPS NLOS effect in highly urbanized area," *GPS Solutions*, vol. 22, no. 1, p. 7, Jan. 2018.

[6] L. Wang, P. D. Groves, and M. K. Ziebart, "Urban positioning on a smartphone: Real-time shadow matching using GNSS and 3D city models," in *Proc. ION GNSS*, Nashville, TN, USA, 2013, pp. 1606–1619.

[7] P. Baranski, M. Polanczyk, and P. Strumillo, "Fusion of data from inertial sensors, raster maps and GPS for estimation of pedestrian geographic location in urban terrain," *Metrology Meas. Syst.*, vol. 18, no. 1, pp. 145–157, 2011.

[8] A. Brilhault, S. Kammoun, O. Gutierrez, P. Truillet, and C. Jouffrais, "Fusion of artificial vision and GPS to improve blind pedestrian positioning," in *Proc. 4th IFIP Int. Conf. New Technol., Mobility Secur.*, Feb. 2011, pp. 1–5.

[9] L.-T. Hsu, Y. Gu, Y. Huang, and S. Kamijo, "Urban pedestrian navigation using smartphone-based dead reckoning and 3-D map-aided GNSS," *IEEE Sensors J.*, vol. 16, no. 5, pp. 1281–1293, Mar. 2016.

[10] S. Godha, G. Lachapelle, and M. E. Cannon, "Integrated GPS/INS system for pedestrian navigation in a signal degraded environment," in *Proc. ION GNSS*, Fort Worth TX, USA, Sep. 2006, pp. 26–29.

[11] Y. Zhao, "Standardization of mobile phone positioning for 3G systems," *IEEE Commun. Mag.*, vol. 40, no. 7, pp. 108–116, Jul. 2002.

[12] G. Retscher and Q. Fu, "Integration of RFID, GNSS and DR for ubiquitous positioning in pedestrian navigation," *J. Global Positioning Syst.*, vol. 6, no. 1, pp. 56–64, Jun. 2007.

[13] J. Ye, J. Li, H. Luo, J. Wang, W. Chen, and Q. Zhang, "Hybrid urban canyon pedestrian navigation scheme combined PDR, GNSS and beacon based on smartphone," *Remote Sens.*, vol. 11, no. 18, p. 2174, Sep. 2019.

[14] J. L. Wilson, "Automotive WiFi availability in dynamic urban canyon environments," *Navigation*, vol. 63, no. 2, pp. 161–172, Jun. 2016.

[15] H. Zou, H. Jiang, Y. Luo, J. Zhu, X. Lu, and L. Xie, "BlueDetect: An iBeacon-enabled scheme for accurate and energy-efficient indoor-outdoor detection and seamless location-based service," *Sensors*, vol. 16, no. 2, p. 268, Feb. 2016.

[16] K. Tabata, H. Konno, K. Tsuno, W. Morioka, A. Nishino, M. Nakajima, and N. Kohtake, "The design of selective hybrid positioning by utilizing accuracy information for indoor-outdoor seamless positioning and verification in Tokyo station," in *Proc. Int. Conf. Indoor Positioning Indoor Navigat.*, Oct. 2015.

[17] C. She, X. Yue, L. Hu, and F. Zhang, "Estimation of ionospheric total electron content from a multi-GNSS station in China," *IEEE Trans. Geosci. Remote Sens.*, vol. 58, no. 2, pp. 852–860, Feb. 2020.

[18] G. Mendoza-Silva, M. Matey-Sanz, J. Torres-Sospedra, and J. Huerta, "BLE RSS measurements dataset for research on accurate indoor positioning," *Data*, vol. 4, no. 1, p. 12, Jan. 2019.

[19] G. S. de Blasio, J. C. Rodríguez-Rodríguez, C. R. Garcia, and A. Quesada-Arencibia, "Beacon-related param of Bluetooth low energy: Development of a semi-automatic system to study their impact on indoor positioning systems," *Sensors*, vol. 19, no. 14, p. 3087, Jul. 2019.

[20] J. Röbesaat, P. Zhang, M. Abdelaal, and O. Theel, "An improved BLE indoor localization with Kalman-based fusion: An experimental study," *Sensors*, vol. 17, no. 5, p. 951, Apr. 2017.

[21] R. Faragher and R. Harle, "Location fingerprinting with Bluetooth low energy beacons," *IEEE J. Sel. Areas Commun.*, vol. 33, no. 11, pp. 2418–2428, Nov. 2015.

[22] R. Chen, "Introduction to smart phone positioning," in *Ubiquitous Positioning Mobile Location-Based Services Smart Phones*. Hershey, PA, USA: IGI Global, 2012, pp. 1–31.

[23] T. Pfau, M. Ferrari, K. Parsons, and A. Wilson, "A hidden Markov model-based stride segmentation technique applied to equine inertial sensor trunk movement data," *J. Biomech.*, vol. 41, no. 1, pp. 216–220, Jan. 2008.

[24] A. Mannini and A. M. Sabatini, "Accelerometry-based classification of human activities using Markov modeling," *Comput. Intell. Neurosci.*, vol. 2011, pp. 1–10, Sep. 2011.

[25] P. Siirtola and H. Röning, "Recognizing human activities user-independently on smartphones based on accelerometer data," *Int. J. Interact. Multimedia Artif. Intell.*, vol. 1, no. 5, pp. 38–45, 2012.

[26] A. Brajdic and R. Harle, "Walk detection and step counting on unconstrained smartphones," in *Proc. ACM Int. Joint Conf. Pervas. Ubiquitous Comput.*, Sep. 2013, pp. 225–234.

[27] K. H. Chu, X. Jiang, and C. Menon, "Wearable step counting using a force myography-based ankle strap," *J. Rehabil. Assistive Technol. Eng.*, vol. 4, Jan. 2017, Art. no. 205566831774630.

[28] X. Jiang, K. H. Chu, and C. Menon, "An easy-to-use wearable step counting device for slow walking using ankle force myography," in *Proc. IEEE Int. Conf. Syst., Man, Cybern. (SMC)*, Oct. 2017, pp. 2219–2224.

[29] J. W. Kim, H. J. Jang, D.-H. Hwang, and C. Park, "A step, stride and heading determination for the pedestrian navigation system," *J. Global Positioning Syst.*, vol. 3, nos. 1–2, pp. 273–279, Dec. 2004.

[30] A. Abadleh, E. Al-Hawari, E. Alkafaween, and H. Al-Sawalqah, "Step detection algorithm for accurate distance estimation using dynamic step length," in *Proc. 18th IEEE Int. Conf. Mobile Data Manage. (MDM)*, May 2017, pp. 324–327.

[31] L. Fang, P. J. Antsaklis, L. A. Montestruque, M. B. Mcmickell, M. Lemmon, Y. Sun, H. Fang, I. Koutroulis, M. Haenggi, M. Xie, and X. Xie, "Design of a wireless assisted pedestrian dead reckoning system—The NavMote experience," *IEEE Trans. Instrum. Meas.*, vol. 54, no. 6, pp. 2342–2358, Dec. 2005.

[32] P. Chen, Y. Kuang, and X. Chen, "A UWB/Improved PDR integration algorithm applied to dynamic indoor positioning for pedestrians," *Sensors*, vol. 17, no. 9, p. 2065, Sep. 2017.

[33] S. Beauregard, "A helmet-mounted pedestrian dead reckoning system," in *Proc. 3rd Int. Forum Appl. Wearable Comput.*, Bremen, Germany, Mar. 2006, pp. 1–11.

[34] P. Goyal, V. J. Ribeiro, H. Saran, and A. Kumar, "Strap-down pedestrian dead-reckoning system," in *Proc. Int. Conf. Indoor Positioning Indoor Navigat.*, Sep. 2011, pp. 1–7.

[35] A. Rai, K. K. Chintalapudi, V. N. Padmanabhan, and R. Sen, "Zee: Zero-effort crowdsourcing for indoor localization," in *Proc. 18th Annu. Int. Conf. Mobile Comput. Netw. Mobicom*, 2012, pp. 293–304.

[36] M.-S. Pan and H.-W. Lin, "A step counting algorithm for smartphone users: Design and implementation," *IEEE Sensors J.*, vol. 15, no. 4, pp. 2296–2305, Apr. 2015.

[37] X. Kang, B. Huang, and G. Qi, "A novel walking detection and step counting algorithm using unconstrained smartphones," *Sensors*, vol. 18, no. 1, p. 297, Jan. 2018.

[38] A. C. Dirican and S. Aksoy, "Step counting using smartphone accelerometer and fast Fourier transform," *Sigma J. Eng. Nat. Sci*, vol. 8, pp. 175–182, Oct. 2017.

[39] N.-H. Ho, P. Truong, and G.-M. Jeong, "Step-detection and adaptive step-length estimation for pedestrian dead-reckoning at various walking speeds using a smartphone," *Sensors*, vol. 16, no. 9, p. 1423, Sep. 2016.

[40] J.-H. Wang, J.-J. Ding, Y. Chen, and H.-H. Chen, "Real time accelerometer-based gait recognition using adaptive windowed wavelet transforms," in *Proc. IEEE Asia Pacific Conf. Circuits Syst.*, Dec. 2012, pp. 591–594.

[41] T. Judd, "A personal dead reckoning module," in *Proc. ION GPS*, Kansas City, MO, USA, 1997, pp. 47–51.

[42] Q. Ladetto, "On foot navigation: Continuous step calibration using both complementary recursive prediction and adaptive Kalman filtering," in *Proc. ION GPS*, Salt Lake City, UT, USA, 2000, pp. 1735–1740.

[43] R. Chen, L. Pei, and Y. Chen, "A smart phone based PDR solution for indoor navigation," in *Proc. 24th Int. Tech. Meeting Satell. Division Inst. Navigat.*, Portland, OR, USA, 2011, pp. 1404–1408.

[44] H. Weinberg, "Using the ADXL202 in pedometer and personal navigation applications," Analog Devices, Norwood, MA, USA, Appl. Note AN-602, 2002, vol. 2, no. 2, pp. 1–6.

[45] S. Y. Cho and C. G. Park, "MEMS based pedestrian navigation system," *J. Navigat.*, vol. 59, no. 1, pp. 135–153, Jan. 2006.

[46] W. Chen, R. Chen, Y. Chen, H. Kuusniemi, and J. Wang, "An effective pedestrian dead reckoning algorithm using a unified heading error model," in *Proc. IEEE/ION Position, Location Navigat. Symp.*, May 2010, pp. 340–347.

[47] K. Sunagawa, L. Hsu, and S. Kamijo, "Pedestrian dead reckoning for mobile phones with magnetic deviation map and GPS accuracy (ITS)," *IEICE Tech. Rep.*, vol. 114, no. 225, pp. 71–76, 2014.

[48] M. J. Caruso, "Applications of magnetoresistive sensors in navigation systems," SAE Tech. Paper 970602, 1997.

[49] L. Klingbeil and T. Wark, "A wireless sensor network for real-time indoor localisation and motion monitoring," in *Proc. Int. Conf. Inf. Process. Sensor Netw. (IPSN)*, Apr. 2008, pp. 39–50.

[50] H. Lan, C. Yu, and N. El-Sheimy, "An integrated PDR/GNSS pedestrian navigation system," in *Proc. China Satell. Navigat. Conf. (CSNC)*, vol. 342, Berlin, Germany, 2015, pp. 677–690.

[51] Z.-A. Deng, G. Wang, Y. Hu, and D. Wu, "Heading estimation for indoor pedestrian navigation using a smartphone in the pocket," *Sensors*, vol. 15, no. 9, pp. 21518–21536, Aug. 2015.

[52] K. Abdulrahim, C. Hide, T. Moore, and C. Hill, "Aiding low cost inertial navigation with building heading for pedestrian navigation," *J. Navigat.*, vol. 64, no. 2, pp. 219–233, Apr. 2011.

[53] U. Steinhoff and B. Schiele, "Dead reckoning from the pocket—An experimental study," in *Proc. IEEE Int. Conf. Pervas. Comput. Commun. (PerCom)*, Mar. 2010, pp. 162–170.

[54] M. Kourogi and T. Kurata, "A method of pedestrian dead reckoning for smartphones using frequency domain analysis on patterns of acceleration and angular velocity," in *Proc. IEEE/ION Position, Location Navigat. Symp. PLANS*, May 2014, pp. 164–168.

[55] J. Yu, Z. Na, X. Liu, and Z. Deng, "WiFi/PDR-integrated indoor localization using unconstrained smartphones," *EURASIP J. Wireless Commun. Netw.*, vol. 2019, no. 1, pp. 1–13, Dec. 2019.

[56] M. Chowdhary, M. Sharma, A. Kumar, S. Dayal, and M. Jain, "Method and apparatus for determining walking direction for a pedestrian dead reckoning process," U.S. Patent 10 302 434 B2, May 28, 2019.

[57] C. Combettes and V. Renaudin, "Walking direction estimation based on statistical modeling of human gait features with handheld MIMU," *IEEE/ASME Trans. Mechatronics*, vol. 22, no. 6, pp. 2502–2511, Dec. 2017.

[58] Q. Tian, K. I.-K. Wang, and Z. Salcic, "A resetting approach for INS and UWB sensor fusion using particle filter for pedestrian tracking," *IEEE Trans. Instrum. Meas.*, vol. 69, no. 8, pp. 5914–5921, Aug. 2020.

[59] D. Feng, C. Wang, C. He, Y. Zhuang, and X.-G. Xia, "Kalman-filter-based integration of IMU and UWB for high-accuracy indoor positioning and navigation," *IEEE Internet Things J.*, vol. 7, no. 4, pp. 3133–3146, Apr. 2020.

H. Luo *et al.*: Integration of GNSS and BLE Technology With Inertial Sensors for Real-Time Positioning in Urban Environments

IEEE *Access*

[60] M. Karimi, M. Bozorg, and A. R. Khayatian, "A comparison of DVL/INS fusion by UKF and EKF to localize an autonomous underwater vehicle," in *Proc. 1st RSI/ISM Int. Conf. Robot. Mechatronics (ICRoM)*, Feb. 2013, pp. 62–67.

[61] J. Si, Y. Niu, J. Lu, and H. Zhang, "High-precision estimation of steering angle of agricultural tractors using GPS and low-accuracy MEMS," *IEEE Trans. Veh. Technol.*, vol. 68, no. 12, pp. 11738–11745, Dec. 2019.

[62] K. Wen, K. Yu, Y. Li, S. Zhang, and W. Zhang, "A new quaternion Kalman filter based foot-mounted IMU and UWB tightly-coupled method for indoor pedestrian navigation," *IEEE Trans. Veh. Technol.*, vol. 69, no. 4, pp. 4340–4352, Apr. 2020.

[63] H. Xiong, J. Tang, H. Xu, W. Zhang, and Z. Du, "A robust single GPS navigation and positioning algorithm based on strong tracking filtering," *IEEE Sensors J.*, vol. 18, no. 1, pp. 290–298, Jan. 2018.

[64] H. Xiong, R. Bian, Y. Li, Z. Du, and Z. Mai, "Fault-tolerant GNSS/SINS/DVL/CNS integrated navigation and positioning mechanism based on adaptive information sharing factors," *IEEE Syst. J.*, vol. 14, no. 3, pp. 3744–3754, Sep. 2020.

[65] S.-H.-P. Won, W. W. Melek, and F. Golnaraghi, "A Kalman/particle filter-based position and orientation estimation method using a position Sensor/Inertial measurement unit hybrid system," *IEEE Trans. Ind. Electron.*, vol. 57, no. 5, pp. 1787–1798, May 2010.

[66] C. Yang, W. Shi, and W. Chen, "Comparison of unscented and extended Kalman filters with application in vehicle navigation," *J. Navigat.*, vol. 70, no. 2, pp. 411–431, Mar. 2017.

[67] A. Martinelli, H. Gao, P. D. Groves, and S. Morosi, "Probabilistic context-aware step length estimation for pedestrian dead reckoning," *IEEE Sensors J.*, vol. 18, no. 4, pp. 1600–1611, Feb. 2018.

[68] E. O. Brigham and R. E. Morrow, "The fast Fourier transform," *IEEE Spectr.*, vol. 4, no. 12, pp. 63–70, Dec. 1967.

[69] Q. Fu and G. Retscher, "Active RFID trilateration and location fingerprinting based on RSSI for pedestrian navigation," *J. Navigat.*, vol. 62, no. 2, pp. 323–340, Apr. 2009.

[70] G. Retscher, M. Zhu, and K. Zhang, "RFID positioning," in *Ubiquitous Positioning Mobile Location-Based Services Smart Phones*. Hershey, PA, USA: IGI Global, 2012, pp. 69–95.

[71] Y. Shi, W. Shi, X. Liu, and X. Xiao, "An RSSI classification and tracing algorithm to improve trilateration-based positioning," *Sensors*, vol. 20, no. 15, p. 4244, 2020.

[72] B. Wang, X. Gan, X. Liu, B. Yu, R. Jia, L. Huang, and H. Jia, "A novel weighted KNN algorithm based on RSS similarity and position distance for Wi-Fi fingerprint positioning," *IEEE Access*, vol. 8, pp. 30591–30602, 2020.

[73] M. J. Feuerstein, K. L. Blackard, T. S. Rappaport, S. Y. Seidel, and H. H. Xia, "Path loss, delay spread, and outage models as functions of antenna height for microcellular system design," *IEEE Trans. Veh. Technol.*, vol. 43, no. 3, pp. 487–498, 1994.

[74] R. Van der Merwe and E. A. Wan, "The square-root unscented Kalman filter for state and parameter-estimation," in *Proc. IEEE Int. Conf. Acoust., Speech, Signal Processing*, May 2001, pp. 3461–3464.

[75] G. Liu and H. Zhu, "EM-FKF approach to an integrated navigation system," *J. Aerosp. Eng.*, vol. 27, no. 3, pp. 621–630, May 2014.

[76] M. Ji, J. Kim, J. Jeon, and Y. Cho, "Analysis of positioning accuracy corresponding to the number of BLE beacons in indoor positioning system," in *Proc. 17th Int. Conf. Adv. Commun. Technol. (ICACT)*, Jul. 2015, pp. 92–95.

YAXIN LI received the bachelor's degree in geomatics engineering from the School of Geodesy and Geomatics, Wuhan University, China, in 2013, and the master's degree from the Department of Land Surveying and Geo-Informatics, The Hong Kong Polytechnic University, Hong Kong, in 2015, where he is currently pursuing the Ph.D. degree. He has a background in indoor positioning and navigation. His research interests include SLAM, indoor 3D modeling, semantic segmentation, and auto BIM generation.

JINGXIAN WANG received the B.S. and M.S. degrees from the Nanjing University of Aeronautics and Astronautics, Nanjing, China, in 2015 and 2018, respectively. He is currently pursuing the Ph.D. degree with the Department of Land Surveying and Geo-Informatics, The Hong Kong Polytechnic University. His research interests include multi-information fusion, indoor position, pedestrian, and vehicle navigation.
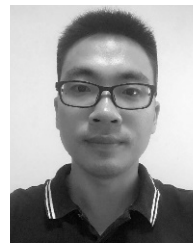
DUOJIE WENG was born in Jiangsu, China, in 1985. He received the B.S. and M.S. degrees in electrical engineering from Hohai University, Nanjing, China, in 2007 and 2010, respectively, and the Ph.D. degree from The Hong Kong Polytechnic University, in 2016. He is currently a Research Associate with The Hong Kong Polytechnic University. His research interests include integrity monitoring of GNSS, kinematic GPS, and sensor integration for various navigation systems.

JUNHUA YE received the master's degree in geodesy and engineering surveying from Chang'an University, in 2012, where he is currently pursuing the Ph.D. degree. His main research interests include GNSS and RO water vapor and multi-sensor fusion navigation.

LI-TA HSU received the B.S. and Ph.D. degrees in aeronautics and astronautics from National Cheng Kung University, Taiwan, in 2007 and 2013, respectively. He is currently an Assistant Professor with the Division of Aeronautical and Aviation Engineering, The Hong Kong Polytechnic University, before he has served as a Postdoctoral Researcher with the Institute of Industrial Science, The University of Tokyo, Japan. In 2012, he was a Visiting Scholar with the University College London, U.K. He is also an Associate Fellow with RIN. His research interests include GNSS positioning in challenging environments and localization for pedestrian, autonomous driving vehicle, and unmanned aerial vehicle.

HUAN LUO received the B.Sc. and M.Sc. degrees in geomatics engineering from Northeastern University, Shenyang, in 2013 and 2015, respectively. She is currently pursuing the Ph.D. degree with the Department of Land Surveying and Geo-Informatics (LSGI), The Hong Kong Polytechnic University. From 2015 to 2016, she was a Research Assistant with the Department of LSGI, The Hong Kong Polytechnic University. Her research interests include GNSS navigation in urban environment and multi-sensor integration for pedestrian navigation.

WU CHEN is currently a Professor with the Department of Land Surveying and Geo-Informatics, The Hong Kong Polytechnic University. He has been actively working on GNSS related research for more than 30 years. His main research interests include GNSS positioning quality evaluation, system integrity, various GNSS applications, seamless positioning, and SLAM.

• • •